Copyright Warning & Restrictions

The copyright law of the United States (Title 17, United States Code) governs the making of photocopies or other reproductions of copyrighted material.

Under certain conditions specified in the law, libraries and archives are authorized to furnish a photocopy or other reproduction. One of these specified conditions is that the photocopy or reproduction is not to be "used for any purpose other than private study, scholarship, or research." If a, user makes a request for, or later uses, a photocopy or reproduction for purposes in excess of "fair use" that user may be liable for copyright infringement,

This institution reserves the right to refuse to accept a copying order if, in its judgment, fulfillment of the order would involve violation of copyright law.

Please Note: The author retains the copyright while the New Jersey Institute of Technology reserves the right to distribute this thesis or dissertation

Printing note: If you do not wish to print this page, then select "Pages from: first page # to: last page #" on the print dialog screen

ABSTRACT

EFFECTS OF HYPERTENSION AND AGING ON VASCULAR SMOOTH MUSCLE CELL CONTRIBUTION TO RECONSTITUTED AORTIC TISSUE STIFFNESS

by
Nancy Lisa Sehgel

Aortic stiffness increases with hypertension and aging, and much of this increase has been thought to occur due to changes in the extracellular matrix. However, an increase in cell stiffness could also be important. To study the cellular contribution to aortic stiffness, a reconstituted aortic tissue model (composed of vascular smooth muscle cells (VSMCs) in a collagen matrix) was developed. VSMCs isolated from thoracic aortic samples of 5-week and 18-week old male spontaneously hypertensive rats (SHR) and normotensive Wistar-Kyoto (WKY) rats were passaged four times and then separately incubated in collagen for two days on a cylindrical mandrel. The resulting tissue rings were subjected to repeated 10% strain steps. The ratio of the steady-state increase of uniaxial stress following the step compared to the 10% strain determined tissue stiffness. This was measured for the intact reconstituted tissue; and following treatment with an actin cytoskeletal disrupter (cytochalasin D), which effectively removed the cellular contribution to stiffness. The cellular contribution was found from the difference between these stiffnesses. Aging and hypertension sharply increased VSMC stiffness (mean ± SEM): 18-week old SHR (1.45 ± 0.17 kPa) showed greater than a 6-fold difference compared to 5-week old SHR (0.24 ± 0.07 kPa), and greater than a 4-fold difference compared to 18- week old WKY (0.33 ± 0.14 kPa). These data suggest that cellular contributions to aortic stiffness may increase with aging and hypertension.

EFFECTS OF HYPERTENSION AND AGING ON VASCULAR SMOOTH MUSCLE CELL CONTRIBUTION TO RECONSTITUTED AORTIC TISSUE STIFFNESS

by
Nancy Lisa Sehgel

A Thesis
Submitted to the Faculty of
New Jersey Institute of Technology
in Partial Fulfillment of the Requirements for the Degree of
Master of Science in Biomedical Engineering

Department of Biomedical Engineering

January 2011

APPROVAL PAGE

EFFECTS OF HYPERTENSION AND AGING ON VASCULAR SMOOTH MUSCLE CELL CONTRIBUTION TO RECONSTITUTED AORTIC TISSUE STIFFNESS

Nancy Lisa Sehgel

Dr. William C. Hunter, Thesis Advisor Professor of Biomedical Engineering, NJIT	Date
Dr. William C. Van Buskirk, Committee Member Distinguished Professor and Chair of Biomedical Engineering, NJIT	Date
Dr. Cheul H. Cho, Committee Member Assistant Professor of Biomedical Engineering, NJIT	Date

BIOGRAPHICAL SKETCH

Author: Nancy Lisa Sehgel

Degree: Master of Science

Date: January 2011

Undergraduate and Graduate Education:

- Master of Science in Biomedical Engineering,
  New Jersey Institute of Technology, Newark, NJ, 2011

- Bachelor of Science in Biomedical Engineering,
  Rutgers University, New Brunswick, NJ, 2008

- Bachelor of Arts in Economics,
  Rutgers University, New Brunswick, NJ, 2008

Major: Biomedical Engineering

This thesis is dedicated to my family who has supported me throughout all of my education.

ACKNOWLEDGEMENT

I owe my deepest gratitude to my thesis advisor, Dr. William C. Hunter, for his guidance in my work and encouragement thus far in graduate school.

Additionally, I would like to acknowledge my committee members Dr. William C. Van Buskirk and Dr. Cheul H. Cho for their tremendously insightful input in my research.

Furthermore, the experimental work conducted for this thesis would not have been possible without the funding and laboratory facilities provided by Dr. Stephen F. Vatner.

Also, I am grateful to Dr. Hongyu Qiu for her technical assistance and mentorship throughout my experimental work.

In addition, I would like to recognize my colleague David Lin for his frequent assistance in the laboratory.

Finally, I am thankful of my family who has always championed my educational aspirations.

TABLE OF CONTENTS

TABLE OF CONTENTS
(Continued)

TABLE OF CONTENTS
(Continued)

LIST OF TABLES

LIST OF FIGURES

LIST OF FIGURES
(Continued)

LIST OF FIGURES
(Continued)

CHAPTER 1

INTRODUCTION

Aortic stiffness is known to increase with aging, and with cardiovascular disease (O'Rourke, 2006). Much of the current understanding of this change has been attributed to changes in concentrations of the extracellular matrix proteins in aortic tissue (Nichols et al., 1998). The goal of this thesis is to investigate another potential source for increased aortic stiffness – changes in vascular smooth muscle cell (VSMC) stiffness.

To measure VSMCs stiffness, a novel approach is utilized. A reconstituted aortic tissue model is created by seeding VSMCs into a collagen matrix to form a tissue construct, in which the cellular stiffness can be distinguished from that of the extracellular collagen matrix (Wakatsuki et al., 2000), (Qiu et al., 2010). Measurement of these mechanical properties is determined from stress-relaxation testing of these tissue constructs.

In particular, the effects of hypertension and aging on VSMC stiffness are considered in this thesis. The VSMCs from two age groups (5-week and 18-week old) of both hypertensive and normotensive male rats are compared. The aim of this thesis is to use the reconstituted tissue model described above to study potential mechanical differences in VSMCs due to hypertension and aging.

1.1 The Significance of Aortic Stiffness

The mechanical properties of the aorta, the largest artery in the systemic circulation, are integral to its physiological function. As the aorta conducts blood ejected from the left ventricle to smaller arteries, it dampens the pressure wave formed by the systolic contraction. The relatively large compliance of the aorta allows it to accommodate the

sudden pulse of blood during systole. Additionally, its ability to elastically recoil helps in pushing the blood forward during diastole, in the absence of an upstream pressure drive, after the aortic valve has closed. The second effect is critical to the heart, since the coronary blood flow that nourishes the myocardium occurs almost exclusively in diastole (Lanzer et al., 2002).

As the aorta conducts the pressure wave forward, a pulse wave is reflected back towards the heart, and this reflected wave which adds to the pressure in the central aorta. In an aorta with normal mechanical properties, the reflected wave reaches the heart during diastole, which adds to the diastolic pressure (O'Rourke, 2006). The pulse pressure (PP), the difference between systolic and diastolic pressures, is proportional to the workload of the heart. Thus, in a normal aorta the reflected waves decrease the PP, which decreases the load on the heart. The increase in aortic pressure during diastole also adds to the driving force that provides perfusion of coronary blood flow to the heart.

The wall stiffness of the aorta is known to increase with age and in cardiovascular disease (Mitchell, 2009). Increased aortic stiffness produces an added strain on the heart for several reasons. A stiffer, and therefore less compliant, aorta does not accommodate as well the ejected blood during systole. Thus, the heart must use more energy to pump blood into a stiffer aorta. Furthermore, increased aortic stiffness leads to an increased pulse pressure wave speed. This is described in the well-known Moens-Korteweg equation.

$$c = \sqrt{\frac{Eh}{\rho d}} \tag{1.1}$$

A faster traveling pulse pressure wave reflects back to the heart sooner in the cardiac cycle. At a sufficient aortic stiffness, the pressure wave can reach the heart during systole, in which case the effective systolic pressure is increased. As a result, the PP is increased, and therefore the workload on the heart.

Increased aortic stiffness may have several detrimental consequences: left ventricular hypertrophy, arterial wall hypertrophy, as well as, increases in the incidence of stroke, kidney disease, coronary artery disease, and heart failure (Safar et al., 2007). Over the past decade, aortic stiffness has become increasingly clinically relevant as a predictor of cardiovascular disease (Mitchell, 2009). Risk factors such as, age, diabetes, obesity, elevated heart rate, hypertension, and lipid disorders, have all been linked with increased aortic stiffness (Mitchell, 2009). Furthermore, it has been suggested that increased aortic stiffness contributes to microcirculation damage. Several microvascular-related conditions common to aging have all been tied to large artery stiffness: cognitive impairment, white matter lesions, macular degeneration, and kidney dysfunction (Mitchell, 2009).

Although the physiological ramifications induced by increased aortic stiffness have been well-recognized, an understanding of the ultimate cellular and molecular processes responsible for this change is limited. Research has progressed in a top-down manner to better understand the causes and development of aortic stiffness.

1.2 Structural Changes in the Aorta due to Increased Stiffness

Arteries are composed of three concentric cellular layers – the outermost *adventitia* consisting of few fibroblast cells, the *media* consisting of spirally organized smooth muscle cells, and the innermost *intima* containing endothelial cells, as shown in Figure

1.1. Additionally, arteries contain two important structural proteins – elastin and collagen – which are the major components of the extracellular matrices (ECMs) found within each layer. Significant amounts of elastin and collagen are found in the media, while the adventia contains mostly collagen (Lanzer et al., 2002).

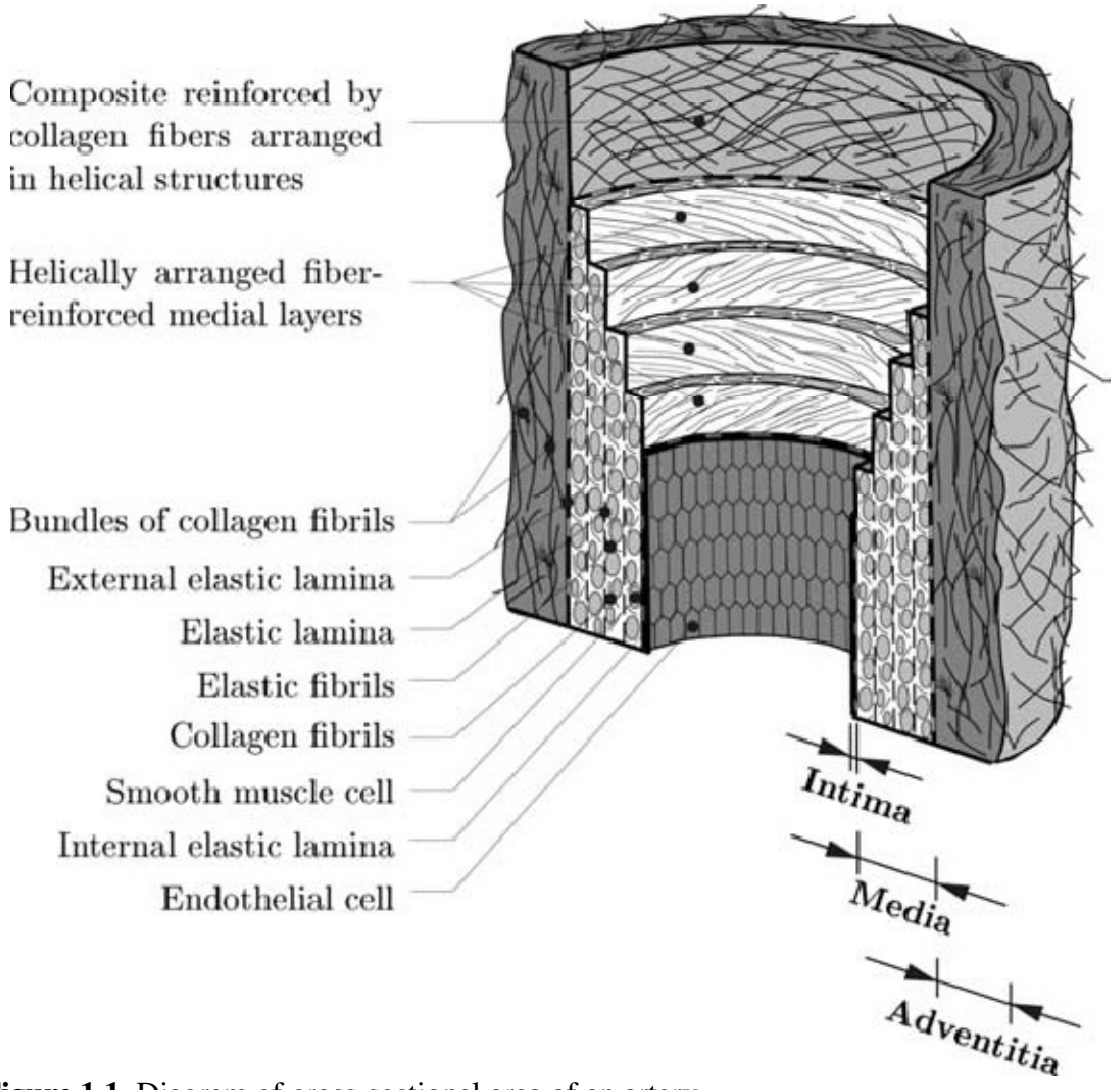

Figure 1.1 Diagram of cross-sectional area of an artery.
Source: (Holzapfel et al., 2000)

The medial layer provides the most significant mechanical properties of the artery. The media is formed by several concentric layers of organized VSMCs, collagen fibrils, and elastin, separated by fenestrated elastic laminae to form a complex three-

dimensional network (Holzapfel et al., 2000). Together, these elastic laminae and the encased VSMCs, collagen, and elastin, form a fibrous helical structure with a small pitch, such that the VSMCs are nearly oriented circumferentially (Holzapfel et al., 2000). This circumferential organization is thought to give the media, and hence the aorta, its strength.

Since the media bears most of the mechanical load within the artery, it is not surprising that increased aortic stiffness is known to be accompanied by several changes in medial morphology. Age related increases aortic diameter and thickness have been both associated with changes on aortic stiffness. This is largely due to the hyperproliferation of VSMCs in the media, known as medial thickening.

Additional changes are known to occur in aortic wall composition have been associated with aortic stiffening. These include age-related breakage of elastin, and replacement by collagen. An example of this medial thickening and elastin fiber breakage is shown in Figure 1.2.

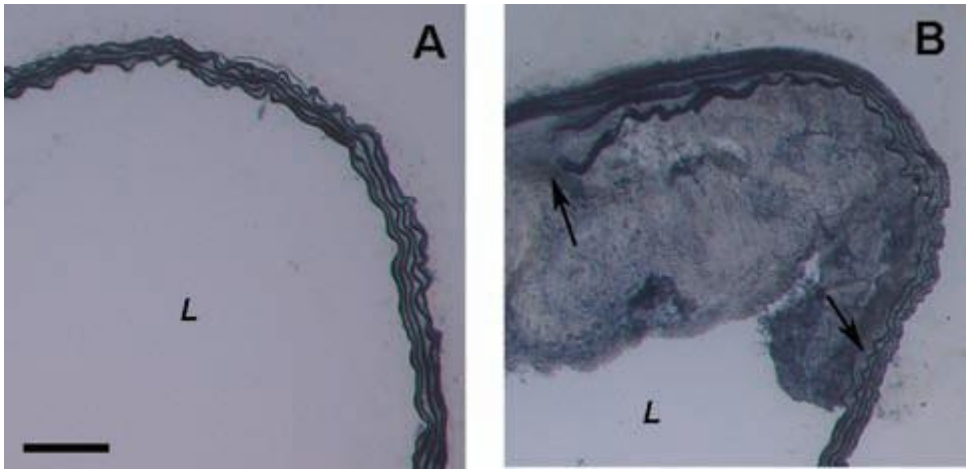

Figure 1.2 A morphological comparison of aortic structure in (A) 8-week old and (B) 34-week old mice. Note the increased medial thickness, and the elastin breakage (indicated by arrows) in (B).
Source: (**S**antelices et al., 2008)

1.3 The Contribution of the ECM to Aortic Stiffness

The relatively large compliance of the aorta is attributed to having the greatest elastin to collagen ratio, as compared to other arteries. This composition enables the unique distensibility of the aorta.

In the normally functioning aorta, the elastin in the media is thought bear much of the load at normal pressures. At higher pressures, more of this load is transferred to the more exponentially stiffening collagen fibers. The benefit of this collagen reinforcement is to prevent ballooning and rupture at higher pressures (O'Rourke, 2006). As a result, the aorta is effectively stiffer at higher working pressures.

Natural changes in theses ECM proteins with age are major contributors to increased aortic stiffness. Elastin is known to fray and fracture. Furthermore, it is thought that over time collagen is recruited to replace this elastin. In a study of 58 human thoracic aortic sections, aged 20 to 78 years old, the ratio of collagen to elastin concentrations in the media was found to increase 2-fold with age (Spina et al., 1983). These changes produce an increase in the total aortic stiffness, similar to the effect of functioning at higher working pressures.

1.4 The Potential for Contribution of VSMCs to Aortic Stiffness

However, other potential factors may contribute to changes in aortic stiffness. A relatively new concept is emerging that mechanical changes in the VSMCs themselves may contribute to increases aortic stiffness.

As motivation for this, consider the cellular-ECM force balance that must exist within the medial layer of the artery. As the structural composition of the ECM changes with age, the extracellular stress is increased on the VSMCs. One method of coping with

this increase in stress is through hyperproliferation of VSMC to decrease the load on individual cells, as described earlier.

Another method may be for individual cells to accommodate this change in the extracellular environment. This may be induced because of a natural lack of spatial uniformity in the VSMC interaction with the ECM. In other words, VSMCs with greater or stronger interactions with ECM proteins may be under greater stresses than those in the same artery with fewer or weaker connections. The VSMCs under greater stresses would have to up-regulate their force exerting capabilities to match that of the extracellular environment.

Conversely, perhaps there are innate differences in the mechanical properties of cells from even the same populations. In this case, inherently stiffer VSMCs may exert greater forces on their extracellular environment. This may cause the changes in the ECM proteins that have been observed with increased aortic stiffness.

This speculation supports by the widely accepted notion that cellular-ECM interactions are bi-directional and dynamic (Palsson et al., 2004). In this thesis it is hypothesized that there may be differences in VSMC stiffness, which could contribute to aortic stiffness.

1.5 VSMC Mechanics

In discussion of the mechanical properties of muscle cells, there is sometimes confusion as to what is meant by cellular force generation. In this thesis, the actin-myosin mechanism of force generation common to muscle cells, is *not* considered. This is the calcium-mediated mechanism that produces the contractile, and in the case of smooth muscle cells, also tonic contraction.

Instead, this thesis is concerned with an unstimulated state (in which, there is no calcium-induced contraction) of VSMCs. However, in both states, the actin-cytoskeletal forces are exerted onto the ECM through integrin proteins.

In general, the cytoskeleton is comprised of three major types of filaments that determine their mechanical properties of the cell – microfilaments, intermediate filaments, and microtubules. Most relevant of these to the scope of this thesis are the microfilaments, which are composed of the monomeric protein actin, which polymerizes to form the network of filaments just beneath the plasma membrane. This actin cytoskeleton adheres to the ECM through the anchoring protein integrin, as shown in Figure 1.3.

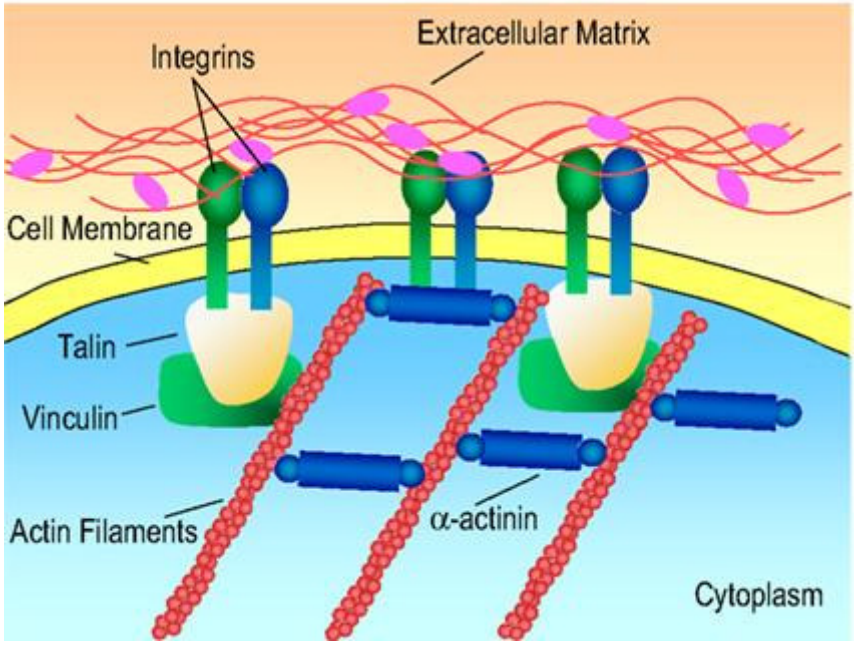

Figure 1.3 Actin filaments bind to the ECM through intregins.
Source: (Rao et al., 2009)

Several techniques have been used to measure the forces produced through the cytoskeleton. One approach is through probing cells using atomic force microscopy (AFM) (Sun et al., 2005).

1.6 Reconstituted Tissue Models as a Approach to Studying Cell-ECM Mechanical Interactions

Alternatively, cellular cytoskeletal mechanical properties can be estimated indirectly through interactions with ECM proteins in three-dimensional bio-artificial tissue constructs. In essence, certain cell types are grown in culture and seeded into ECM-mimicking scaffolds to create model constructs that simulate particular features of the whole tissue environment. These simplified systems, containing only the desired tissue features, are more controlled than whole tissues, which have the added complexities of tissue elements not of interest.

In general, the advantages of studying engineered tissue over whole tissue are numerous. Since the source of cells used for the bio-artificial tissue typically comes from a population of *in vitro* cultured cells, which may be more homogenous than that existing in whole tissues, there is less cellular undesired variability. However, caution must be taken because cultured cells often have altered phenotypic expressions with each successive generation of cells. Thus, the cellular characteristics of the tissue construct may be different than that found from the whole tissue. However, this drawback can be potentially mitigated by performing phenotyping assays to ensure that successive generations are similar. Furthermore, the relative economy of cells used in tissue models, as opposed to whole arteries reduces the number of animals needed for experimentation.

In particular, three-dimensional models offer a more realistic approach to studying cellular-ECM mechanical interactions. Cellular structure is known to be fundamentally different when evaluated in two-dimensional systems. The patterns of mechanical stimuli conveyed to cells are sensitive to the organization of their surrounding

matrix (Griffith et al., 2006). This may due to the fact that three-dimensional systems offer a more natural environment for testing the mechanics of cells because they allow for greater cellular cytoskeleton – matrix interaction (Marquez et al., 2010).

Measurements of the elastic stiffness of these engineered tissue constructs can be made to estimate their relative mechanical differences. This information can be interpreted to determine the extent to which the cells of interest interact with ECM proteins to remodel the tissue (Wakatsuki et al., 2000). Previous studies have used this type of approach to investigate the fibroblast-matrix interactions prevalent in wound healing and tissue development (Bell et al., 1979, Grinnel, 1994). Thus, *in vitro* three-dimensional tissue models, comprised of only specific reconstituted cells and ECM protein components, are simplified model systems that can be used for studying the mechanics of cell-matrix interactions.

In previous studies published by collaborators, a novel method was developed to differentiate between forces exerted by the cellular and ECM components of uni-axially stressed reconstituted tissue models (Wakatsuki et al., 2000). In these studies, fibroblasts were seeded into monomeric collagen solutions to form a cell-collagen suspension, which was poured into cylindrical molds, and incubated at 37°C. After 2 days, the fibroblasts compressed the collagen to form ring-shaped fibroblast-collagen tissue constructs of a gel-like consistency.

Each tissue ring was then looped about a wire hook connected to an isometric force transducer and about a sliding element that could be gradually moved with a stepper motor, similar to the apparatus displayed in Figure 1.4.

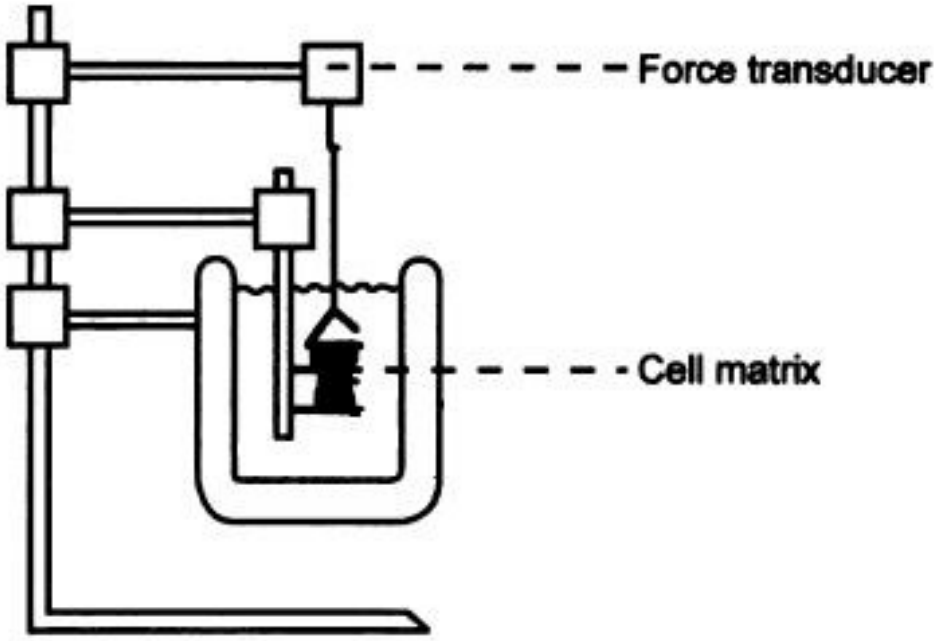

Figure 1.4 Mechanical testing apparatus showing the placement of the tissue construct in relation to the force transducer.
Source: Modified from (Eschenhagen et al., 1997).

The motor drive was then used to gradually and cyclically stretch and unload the tissue rings up to a 20% strain. The viscoelastic force response of the fibroblast-collagen tissue ring was recorded through a data acquisition software, and after two stretching cycles, the force response was considered repeatable. The fibroblast-collagen tissue ring was then treated with cytochalasin D, an actin cytoskeleton disruptor commonly used by cell biologists, to abolish the force-exerting capabilities by the fibroblasts. The tissue ring was subsequently cyclically stretched and recorded again, where only the ECM could exert force. This force response from this last stretch, considered the "passive" force,

was subtracted from that previously recorded before cytochalasin D treatment, termed the "total" force, to determine the cellular contribution, named the "active" force. It was assumed that the fibroblast cells can exert forces only through the actin cytoskeleton. A plot of these force responses as a function of strain is shown in Figure 1.5.

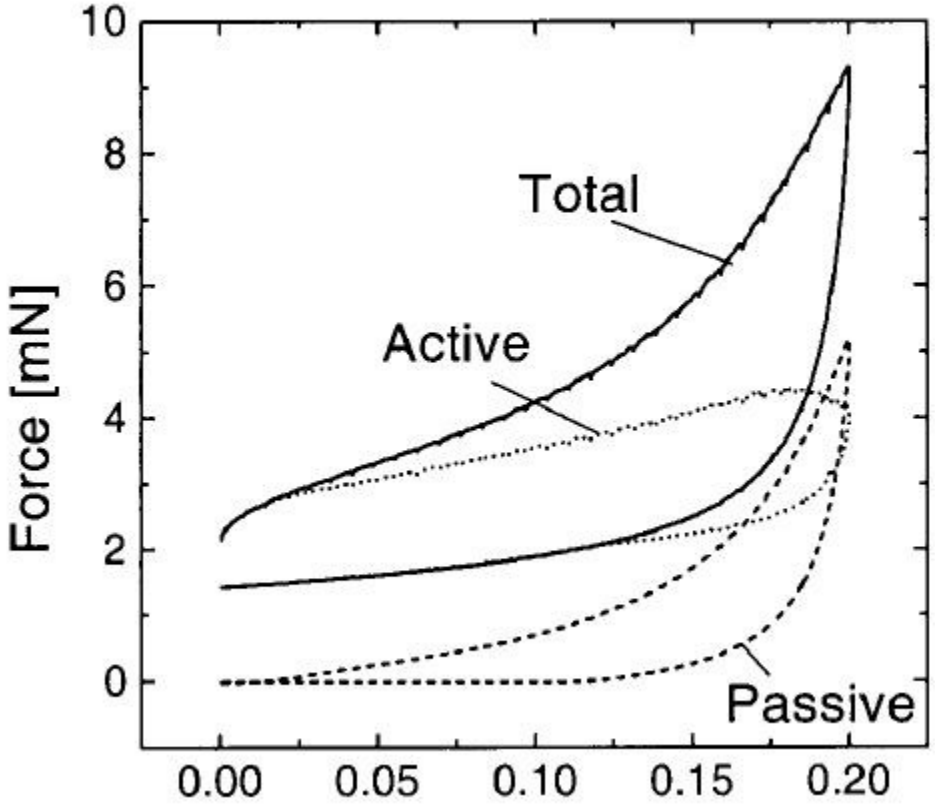

Figure 1.5 Total (cellular and ECM), passive (ECM only), and active (cellular only) forces as a function of strain during cyclic uni-axial stress testing.
Source: Modified from (Wakatsuki et al., 2000).

Measurements of the cross-sectional area and the force recordings could then be used to compute the elastic moduli associated with the total tissue (cellular and ECM), passive (ECM only), and active (cellular only) stiffnesses.

Important findings of the authors include that the magnitude of the cellular elasticity was found to be greater than that of the collagen-containing ECM. Additionally, it is important to note from Figure 1.3 that, at lower strains, the cellular contribution to total tissue stiffness dominates that of the ECM.

This thesis aims to utilize this experimental approach to measure the potential VSMC contributions to tissue stiffness. Tissue constructs will be created using VSMCs and collagen to form simplified models of the medial layer of aortic tissue. Although *in vivo* medial tissue contains significant amounts of elastin, this protein was not included in these artificial tissue constructs in order to create as simple a model as possible. (As it turned out, the presence of collagen only did not adversely produce such a stiff tissue construct.) The mechanics of VSMC and collagen interaction can be studied through uni-axial stress testing. The ability to quantitatively measure the VSMC contribution to tissue stiffness can allow for comparisons of this property amongst animals with different expected aortic stiffnesses, such as with hypertension and aging.

1.7 Spontaneously Hypertensive Rat as an Animal Model of Hypertension

The spontaneously hypertensive rat (SHR) is a commonly used animal model of hypertension. The SHR belongs to a group of phenotypic-driven hypertension models, a subset of the class of genetic models, as described by Figure 1.6.

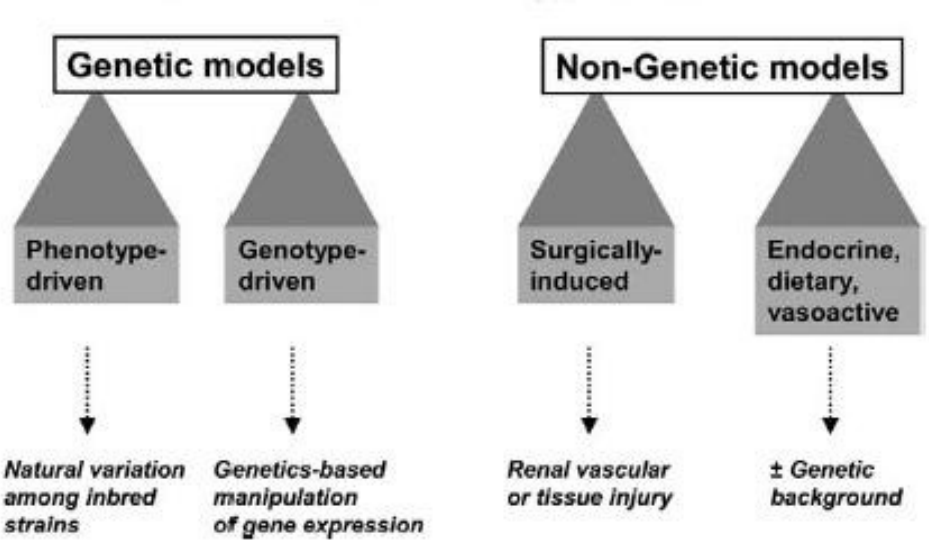

Figure 1.6 Classification of animal models of hypertension.
Source: (Lerman et al., 2005)

These phenotypic models constitute animal models in which the expressed hypertension phenotype may be caused by a variable number of genes (Lerman et al., 2005). For this reason, the SHR is considered a good model of primary hypertension, due to its complex genetic etiology (Lerman et al., 2005). This stands in contrast to other genetic models, in which particular genes are manipulated to study their roles in hypertension (Lerman et al., 2005). Furthermore, the class of genetic models is different from the class of non-genetic models, in which hypertension is induced by through surgical, endocrine, dietary, or vasoactive methods (Lerman et al., 2005). These models are appropriate for studying secondary hypertension, in which the elevated blood pressure is due to a secondary cause (Lerman et al., 2005).

The SHR strain of rat was developed by Okamoto and colleagues at the Kyoto School of Medicine of Japan in 1963 (Okamoto, 1963). A male Wistar-Kyoto (WKY) rat with high blood pressure (150-175 mmHg) was mated to a female WKY with moderately high blood pressure (130-140 mmHg) to produce some offspring with hypertension

(blood pressure of at least 150 mmHg recorded for over a month). These rats were cross-breed to produce several subsequent hypertensive generations, which were again selected for continued inbreeding. Many of the rats showed a spontaneous development of hypertension, and the age of incidence of hypertension decreased with each generation. On average, male rats had a blood pressure of 10.6 mmHg higher than females of the same age, and developed hypertension at earlier ages than the females. These rats were considered to constitute a new strain called the SHR.

The SHR was introduced to the NIH in 1966 at the thirteenth generation of offspring, and eventually to Charles River Laboratories, a major distributor of animal models in the United States, in 1973 at the thirty-second generation (Charles River Laboratories, Inc., 2010). Charles River has conducted studies to characterize the degree of hypertension with age of their SHR population. Blood pressure recordings of male SHR are shown in Figure 1.7.

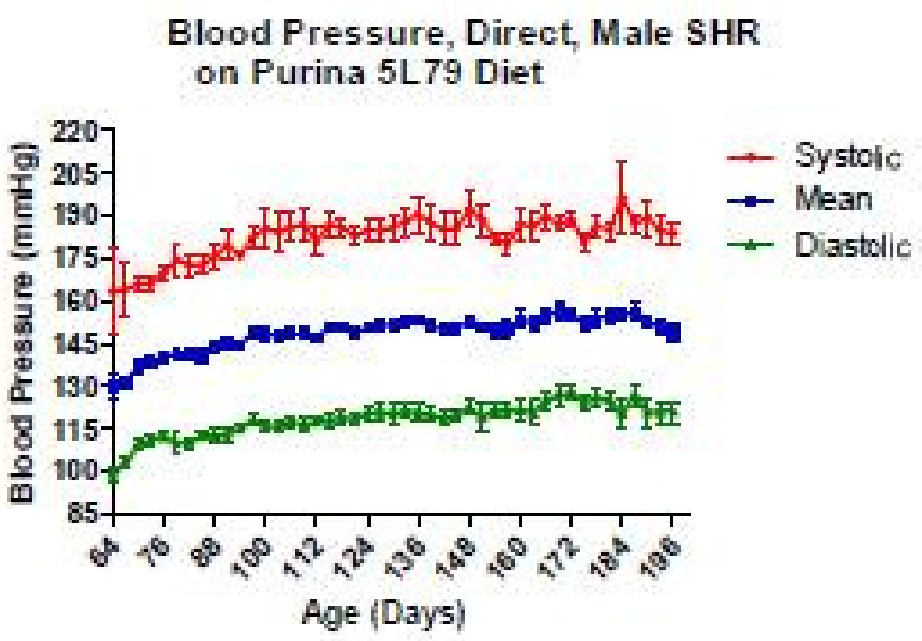

Figure 1.7 Average blood pressure recordings of male SHR (n = 8) from age 9 to 28 weeks.
Source: (Luo et al., 2008)

By comparison, blood pressure readings for the male normotensive control WKY are shown in Figure 1.8.

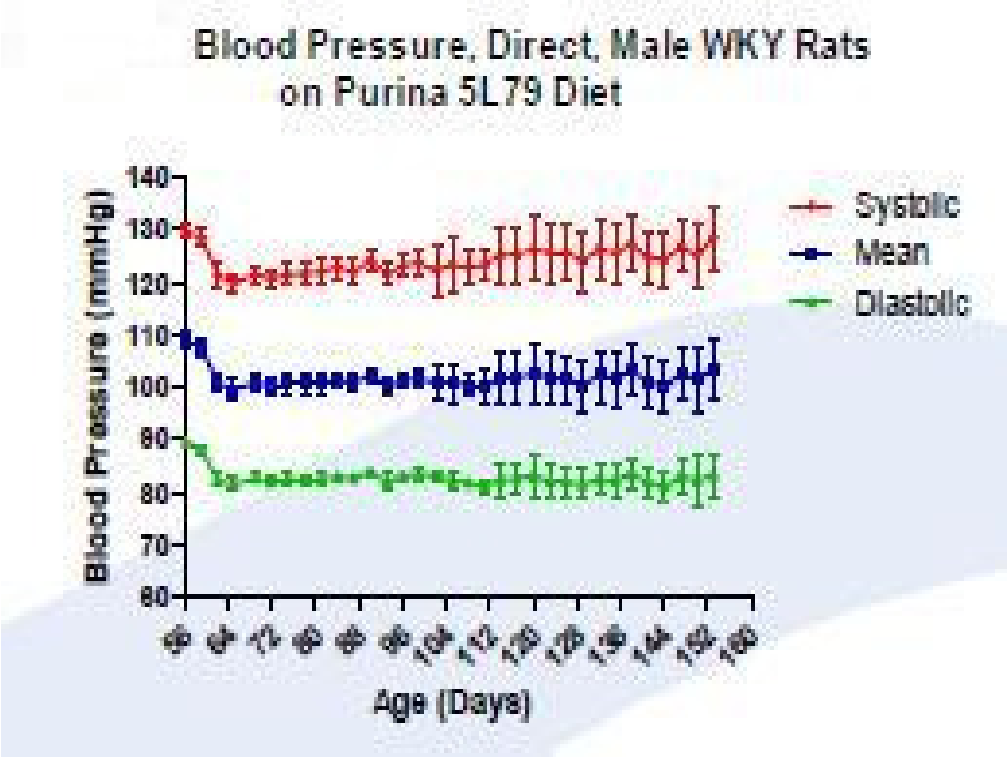

Figure 1.8 Average blood pressure recordings of male WKY (n = 4) from age 7 to 22 weeks.
Source: (Luo et al., 2008)

In both cases, blood pressure was recorded through surgical insertion of a surgically implanted telemetry device (Luo et al., 2008). Figure 1.2 shows that the initial slightly elevated blood pressure of the WKY decreased to about normal after the first week, which experimenters attribute to recovery from surgery (Luo et al., 2008). Blood pressure rises, albeit slowly, to become slightly elevated in later ages. By contrast, Figure 1.1 shows an already hypertensive average blood pressure of 164 mmHg at 9 weeks of age increase of 3.5 mmHg per week up until it plateaus at 16 weeks of age, averaging 187 mmHg throughout the rest of the 28 weeks (Luo et al., 2008).

Other studies have demonstrated hypertension in SHR in as young as 5 weeks old that increases with age (Chamiot-Clerc et al., 2001). The mean arterial pressure (MAP) of SHR and its control WKY at 5, 12, 52, and 78 weeks is shown in Figure 1.9.

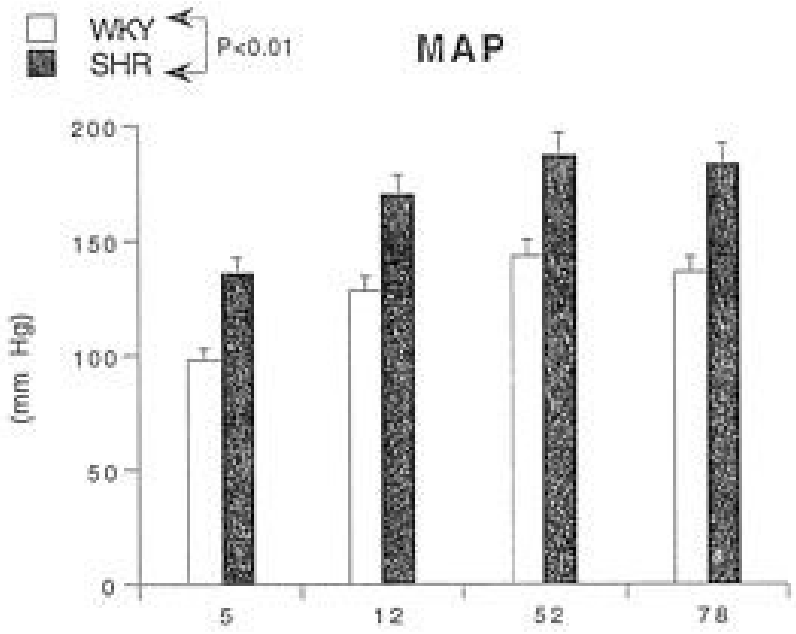

Figure 1.9 Mean arterial pressure of SHR and WKY at various weeks of ages.
Source: (Chamiot-Clerc et al., 2001)

The MAP of both SHR and WKY were found to increase with age, with the SHR showing higher pressures in each age group (Chamiot-Clerc et al., 2001).

Additionally, many of the structural changes associated with aortic stiffness in hypertension and aging in humans have been demonstrated in comparative studies of SHR and WKY. Studies of 3-, 9-, and 15-month old SHR and WKY show increased internal thoracic aortic diameter and medial thickness with age (Marque et al., 1999). This was attributed to age-related dilation, as the medial thickness/internal diameter ratio remain constant for with age, though was found higher in SHR (Marque et al., 1999). This implies that increased aortic stiffness is not merely due to structural changes, but a

change in the material properties of the aorta (Safar et al., 2001). In fact, the Moens-Korteweg equation was applied in this study to determine that the elastic modulus of the thoracic aorta changes dramatically with age in SHR but not WKY, for which no significant change with age was seen (Marque et al., 1999).

Additional studies have shown aortic histomorpholgical changes in SHR that parallel human aortic response to hypertension and aging. Increased medial cross-sectional areas, collagen content, and collagen/elastin ratios were shown to increase with age in 3- to 78- weeks of age SHR and WKY; these values were significantly higher in the SHR (Chamiot-Clerc et al., 2001). Furthermore, the elastin content of the aortas was found to decrease with age in both SHR and WKY strains (Chamiot-Clerc et al., 2001).

Of course, the SHR does not perfectly mimic human response to hypertension and aging. Limitations of the SHR include a lack of ability to develop the hypertension complications prevalent in humans: atherosclerosis, myocardial infarction, aneurysm, or heart failure (Lerman et al., 2005). Additionally, since the development of hypertension is much more accelerated in the SHR than in humans, caution must be made when extrapolating conclusions drawn from experiments with this model to humans. However despite these potential drawbacks, the strong phenotypic similarities displayed by the SHR underlie its strengths as an animal model of hypertension.

In this thesis, the SHR and WKY are used as models of hypertension and aging. Two age groups are considered: 5-week and 18-week. This combination of ages was chosen such that, at the younger age, hypertension has not fully developed in the SHR (Figure 1.9), and at the older age, hypertension is maximal and comparable to that recorded in humans (Figure 1.7). Important to note is that it is unsure how the 5-week

SHR will compare to the older WKY, since moderate blood pressure elevation has been shown in each (Figure 1.9 and Figure 1.8).

1.8 Thesis Objectives

Aortic stiffness has been identified as a significant factor in cardiovascular health. Increased stiffness impairs physiological function of the aorta, and has been implicated with several cardiovascular disease risk factors, in particular, aging and hypertension. The SHR and its normotensive control, the WKY, provide adequate animal models by which to study aortic changes under those conditions.

Current research concerns the fundamental source of aortic stiffness. Age-related changes found in the media layer or the aorta – essentially comprising VSMCs and the ECM proteins elastin and collagen – are thought to increase aortic stiffness. Much of the present understanding in the development of increased aortic stiffness is attributed to these changes in the ECM. However, little is known of the possible role VSMCs themselves and interactions between VSMCs and ECM may have in altering aortic stiffness.

The objective of this thesis is to determine a potential cellular contribution to tissue stiffness using VSMCs derived from the thoracic aortas of SHR and WKY animals. This is accomplished by using the reconstituted cell-collagen tissue model described earlier, in which, the active cellular stiffness can be distinguished from that of passive ECM. These constructed tissues are presented as simplified systems of the VSMC-ECM interaction in aortic tissue. The mechanical properties of the tissues will be determined from uni-axial stretch measurements. Ultimately, the hope is to be able to extrapolate any mechanical differences found between these experimental tissues to that which could

occur in the native aorta. The reconstituted tissue model may offer a more highly controlled experimental test of the role that VSMCs contribute to aortic stiffness.

CHAPTER 2

METHODS

VSMCs from two different strains were used to construct representative arterial tissue models that could be mechanically stressed and compared based on their experimentally determined elastic moduli. The specifics of experimental approach were similar to that described previously by other biomedical engineering collaborators (Wakatsuki et al., 2000).

The experimental work consisted of four phases. The first step was to fabricate the tissue models using the VSMCs originating from aortic tissue segments harvested from the chosen experimental animal strains at the chosen ages. Next, these tissue models were subjected to uni-axial stress testing, which utilized a protocol based on the laboratory's already available mechanical testing apparatus. Thirdly, the tissue models were treated pharmacologically to remove the cellular contribution to the tissue elastic stiffness. Lastly, data from the time course of force response during the mechanical testing was digitally filtered and analyzed to compute tissue elastic moduli.

2.1 Biological Sample Preparation

The constructed tissue models used for experimentation were fabricated using VSMCs isolated from the thoracic aortas of two strains of experimental animals: SHR and their normotensive control, WKY. Male rats of two age groups, 5- and 18-weeks old, were purchased from Charles River and maintained at the University of Medicine and

Dentistry of New Jersey, Newark (UMDNJ) animal care facilities and in compliance with 3the Guide for the Care and Use of Laboratory Animals (National Institutes of Health 83-23, revised 1996).

2.1.1 Harvesting Aortic Tissue and Subsequent Isolation of VSMCs

The animals were anesthetized and euthanized in accordance with protocols approved by the Institutional Animal Care and Use Committee of UMDNJ. An approximately 2 cm long segment of the thoracic aorta of each animal was dissected and rinsed in phosphate buffered saline (PBS). The segment was then placed in a 60 mm x 15 mm Petri dish containing 5 mL of PBS. The outer layer, adventitia, and inner layer, intima, were removed using forceps. The remaining medial layer containing the VSMCs was placed in another 60 mm x 15 mm culture dish and divided into smaller sections, about 1 mm in length, which were covered in Vascular Smooth Muscle Cell Growth Medium. Finally, all of the tissue culture dishes were placed in a 37 °C incubator with 5% CO_2.

These tissue culture dishes were examined daily under a 4X objective optical microscope to observe resettlement of the VSMCs from aortic issue segments to the floor of the culture dish. Once a significant number of these primary VSMCs had dissociated from the tissue, the tissue and cells were cultured separately. The remaining aortic tissue was transferred to another 100 mm x 20 mm culture dish and incubated in medium as described previously.

The VSMCs were subsequently transferred to another culture dish. First the adherent VSMCs needed to be lifted from the original floor of the culture dish surface. To accomplish this, the remaining medium was aspirated and the bottom surface of the tissue dish was rinsed with 2 mL of warmed 0.05% trypsin-EDTA. This was quickly

aspirated and replaced by another 3 mL of 0.05% trypsin-EDTA. The culture dish was then placed in the incubator for 10 minutes. Afterwards, the culture dish was removed from the incubator and examined under a 4X objective to observe that the VSMCs were no longer adhering to the culture dish and were floating in the 0.05% trypsin-EDTA suspension. Subsequently, 5 mL of culture medium was added to the dish. The resulting solution was transferred to a 15 mL centrifuge tube and spun in a centrifuge at 1000 rpm for 5 minutes. The overlying supernatant was aspirated and 1 mL of culture medium was added to the resulting pellet containing the VSMCs. This suspension was added to a 100 mm x 20 mm culture dish containing 9 mL of culture medium, which was subsequently placed in the incubator.

This procedure was repeated as often as cells were observed to leave the tissue sample; there were usually only 1-2 repetitions.

2.1.2 Passaging of the VSMCs

In order increase the supply of cells as needed for experimentation, as well as to create a backup source of cells, the cells obtained from the dissected tissue were repetitively and sequentially allowed to multiply, and subsequently passaged, or separated to form a new generation of cells. First, the cells isolated directly from the aortic tissue were allowed to proliferate until they were sufficiently confluent, whereby they covered 90% of the area of the culture dish. Once this stage was reached, the population of VSMCs was removed from the dish as described previously, and divided into three portions, which provided the first generation of VSMCs. One portion of the VSMCs in this first generation was transferred to another 100 mm x 20 mm culture dish where it was allowed to continue to proliferate until confluence was reached again.

The remaining two portions were separately frozen. This was achieved by aspirating the supernatant and re-suspending the cells in 2 mL of a freezing medium (a filtered solution 70% Dulbecco's Modified Eagle Medium (DMEM), 30% fetal bovine serum (FBS), and 10% dimethyl sulfoxide (DMSO)). Aliquots of the suspension were divided amongst two 1 mL cryogenic vials. These vials were then placed on ice for 20 minutes, and then stored in a -80°C freezer as a reserve for the first generation of cells.

As necessary, the frozen VSMCs were thawed and re-plated for continued proliferation of the particular cell line. This was done by thawing the cryogenic vial in a 37°C incubator. The contents of the vial were added to 4 mL of the freezing medium described above and centrifuged at 1000 rpm for 5 minutes. The supernatant was aspirated, and the VSMCs-containing pellet was re-suspended in 1 mL VSMC Growth Medium. This suspension was then added to a 100 mm x 20 mm culture dish containing 9 mL of VSMC Growth Medium.

The VSMCs were passaged three more times - for a total of four passages. During each of these subsequent passages, the nearly confluent plate of cells was split into three groups. One of these groups was then subsequently cultured to expand the number of cells for the next generation, while the other two were frozen according to the method described above. Passaging was stopped with the fourth generation of cells, which was used for experimentation.

2.1.3 Formation of the Tissue Model

An experimental aortic tissue model was formed by separately culturing VSMCs from each animal strain in a gel suspension of collagen and DMEM on a cylindrical mold, according to a protocol previously established by collaborators (Wakatsuki et al., 2000).

After a two-day incubation period, the resulting cellularized ring-shaped tissue could be removed from the mold and used for biomechanical testing. The procedure to create these tissue rings is discussed in the following paragraphs.

First, the VSMCs were obtained from the culture dish and the concentration of cells was approximately measured, as explained next. The fourth generation of VSMCs was first separated from its culture dish by rinsing and incubating the cells in 0.05% trypsin-EDTA, as described above. Approximately 5 mL of VSMC growth medium was added to this solution, and the resulting mixture was centrifuged at 1000 rpm. The supernatant layer was aspirated off, and the VSMC pellet was re-suspended in 1 mL of DMEM. A 3 μL sample of this cell-containing suspension was removed and diluted in 27 μL of DMEM (1:10 dilution in DMEM). Drops of this dilution were placed on a hemocytometer for counting under the 10X objective of an optical microscope. The average number of cells within previously chosen gridlines on the hemocytometer was determined. This average number of cells reflected a diluted sample (1:10) concentration on the order of 10^5 cells/mL, and thus a cell concentration (CC) on the order of 10^6 cells/mL. The minimum CC that had to be achieved to adequately seed the reconstituted tissue was 1.2×10^6 cells/mL.

Once the concentration of VSMCs was known, it was used to calculate the amounts of cell solution, collagen, and medium needed to form the tissue ring models. For each experiment, 1 mL of VSMC-containing gel suspension was created. Preliminary experimentation determined that 7.5×10^5 cells VSMCs were required to successfully form tissue gel that had a volume of 1 mL. This number was divided by the approximate CC to determine the volume of cell suspension (in DMEM) needed. This

volume was added to a new 15 mL centrifuge tube. The remaining cell suspension was added to 9 mL of VSMC growth medium and re-plated in a 100 mm x 20 mm culture dish for use in forming subsequent tissue models.

It was determined from previous work (Wakatsuki et al., 2000) that approximately 1 mg of collagen was needed for the 1 mL of gel to be formed. Given the 5.26 mg/mL stock concentration of rat tail monomeric type I collagen, used in this study, 190 μL of stock collagen solution was needed for each tissue gel. The collagen was supplemented with an equal volume of 2X DMEM (DMEM with twice the concentration of nutrients). Finally, enough standard DMEM was added so that the final volume of the gel suspension was 1 mL. The final volumes of VSMC suspension, collagen, and medium are summarized below in Table 2.1.

Table 2.1 Volumes Needed of Tissue Gel Components

Tissue Gel Component	Volume Needed
VSMC suspension	(7.5×10^5 cells)/ CC *
Collagen	190 μL
2X DMEM	190 μL
DMEM	1000 μL – volumes of VSMC suspension, collagen, and 2X DMEM
Total	1000 μL

* This is the volume of suspension needed to collect 7.5×10^5 cells so that the final tissue construct had a cell density of 7.5×10^5 cells/mL. Thus, a minimum CC of 1.2×10^6 cells/mL were needed to form a tissue construct.

The tissue models were constructed using four cylindrical Teflon molds, shown in Figure 2.1. Each mold consisted of an outer cylindrical tube (inner diameter = 7 mm),

and an inner cylindrical mandrel (diameter = 4.5 mm), which were held together with a screw. There was thus a 1.25 mm space between mandrel and tube, which formed the space for the tissue ring. Before contact with the biological specimen, the disassembled molds and a screw driver were sterilized in an autoclave for 40 minutes at 180 °C and 15 psi. After autoclaving, the molds were transferred to the sterile biological safety hood, where they were assembled in a sterile region. Four molds were available, so four rings were prepared at the same time.

Figure 2.1 The four cylindrical tubes and mandrels used to form the tissue rings.

The prepared tissue gel suspension was then divided amongst the four tissue molds and allowed to incubate. A 200 µL modicum of thoroughly mixed solution was placed in each tissue mold. The set of four tissue molds each containing tissue solution was subsequently placed into the incubator (37 °C and 5% CO_2) to congeal for 1 hour. During this time, the VSMCs compressed the collagen, thereby thickening and

solidifying the tissue suspension. Afterwards, the tissue molds were removed from the incubator to be filled to capacity with DMEM, and then returned to the incubator. The tissue molds were left to incubate for 2 more days, with evaporated DMEM replaced after the first day. After this period of incubation, a tissue ring was formed on the inner mandrel of the tissue mold and was used for experimentation. This procedure for preparation of the tissue rings is summarized in Figure 2.2 on the next page. Although this figure shows the protocol using fibroblast cells, it is similar to that with VSMCs.

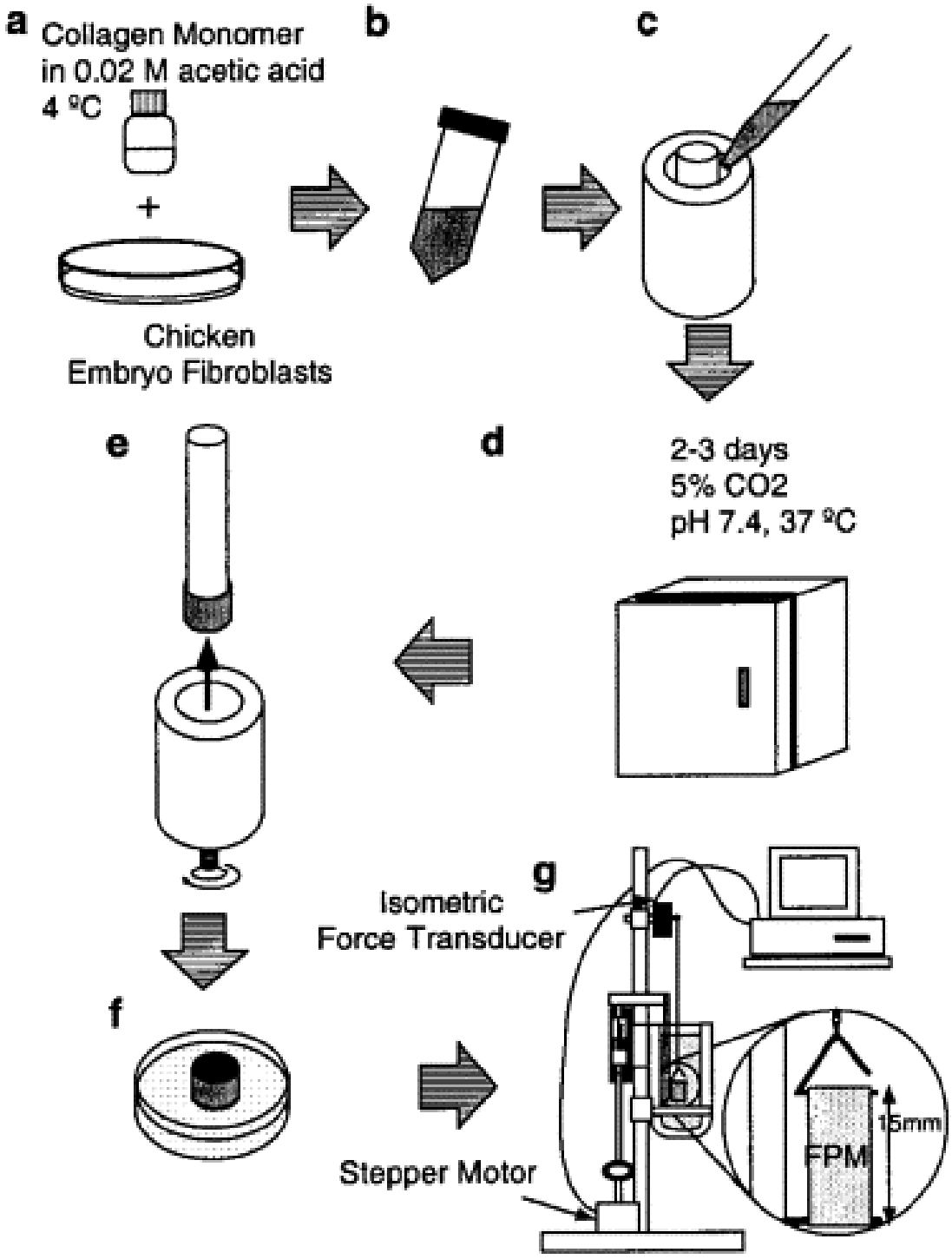

Figure 2.2 An illustration of the procedure used to construct and biomechanically test the tissue ring models.
Source: (Wakatsuki et al., 2000)

2.1.4 Measuring the Dimensions of the Tissue Rings

It was imperative to measure the dimensions of the VSMC tissue rings in order to calculate the stress generated while they were stretched, as well as make size comparisons. While the tissue remained on the mandrel, its axial extent was rapidly measured using calipers. (This axial extent was later related to the width of the tissue ring when it hung on the mechanical testing apparatus.) The tissue was then briefly placed on an inverted microscope with a 2X objective connected to a digital camera. This thickness of each tissue was measured indirectly from the number of pixels in the produced image and comparing it to a known calibration. The image was imported into MATLAB, in which the Image Processing Toolbox allowed for interactive visual determination of the thickness. The number of pixels of this selection was displayed, and the thickness measurement was taken. This process is shown in Figure 2.3.

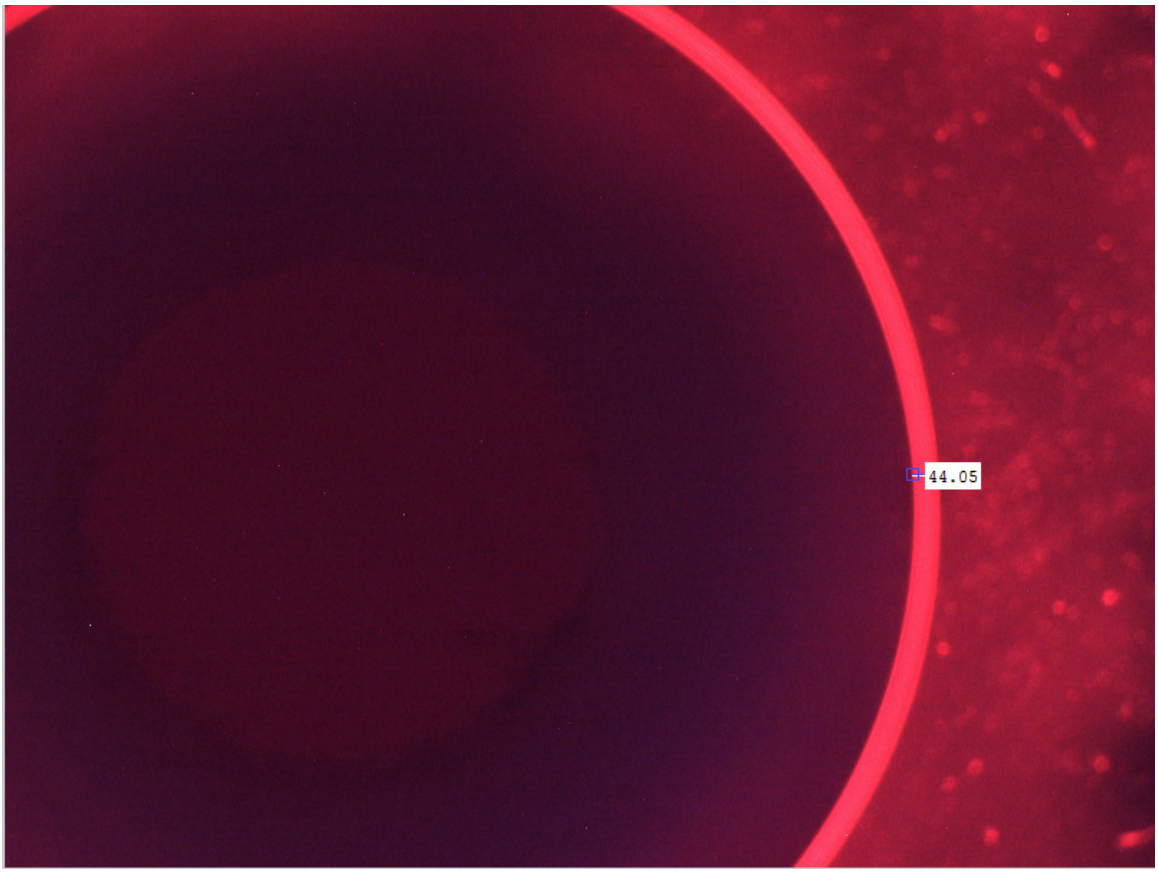

Figure 2.3 Visual determination of the thickness using the pixel distance tool in the Image Processing Toolbox in MATLAB. Note this image was taken under a red filter.

These measurements taken on the mandrel, the axial extent and the thickness, while the ring was not in a medium bath, were measured quickly to minimize dehydration of the tissue ring.

After separating the tissue from the mandrel using pipette-controlled, low pressure jet liquid pressure of DMEM, the ring was transferred into a 60 mm x 15 mm culture dish containing 4 mL of DMEM. Once off the mandrel, the tissue ring expanded and flattened out. Approximations of the width and length of the tissue were made by placing calipers underneath the culture dish to gauge each ring's length and width measurements, which are illustrated in Figure 2.4.

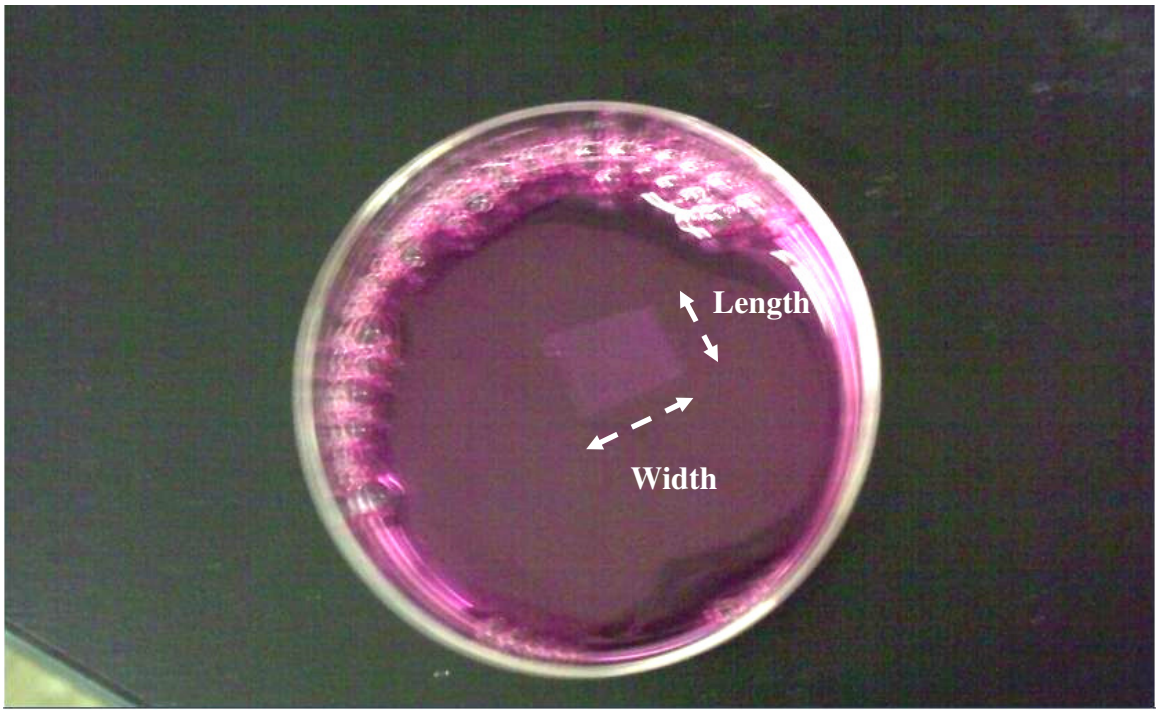

Figure 2.4 Length and width dimensions of the unloaded, flattened tissue ring.

2.2 Mechanical Testing Apparatus

The tissue rings were subject to mechanical testing using an isometric force transducer and a manually controlled micrometer drive system, shown in Figure 2.5. The apparatus could produce and hold sudden stretches of the tissues, and was thus suitable for stress-relaxation testing. The mechanical system was adjusted to produce the stress-relaxation stretching parameters, which were chosen based on the dimensions of tissue rings. Data from the forces exerted onto the force transducer were output to a computer concurrently running a data acquisition software (NOTOCORD Systems SAS, Croissy-sur-Seine, France).

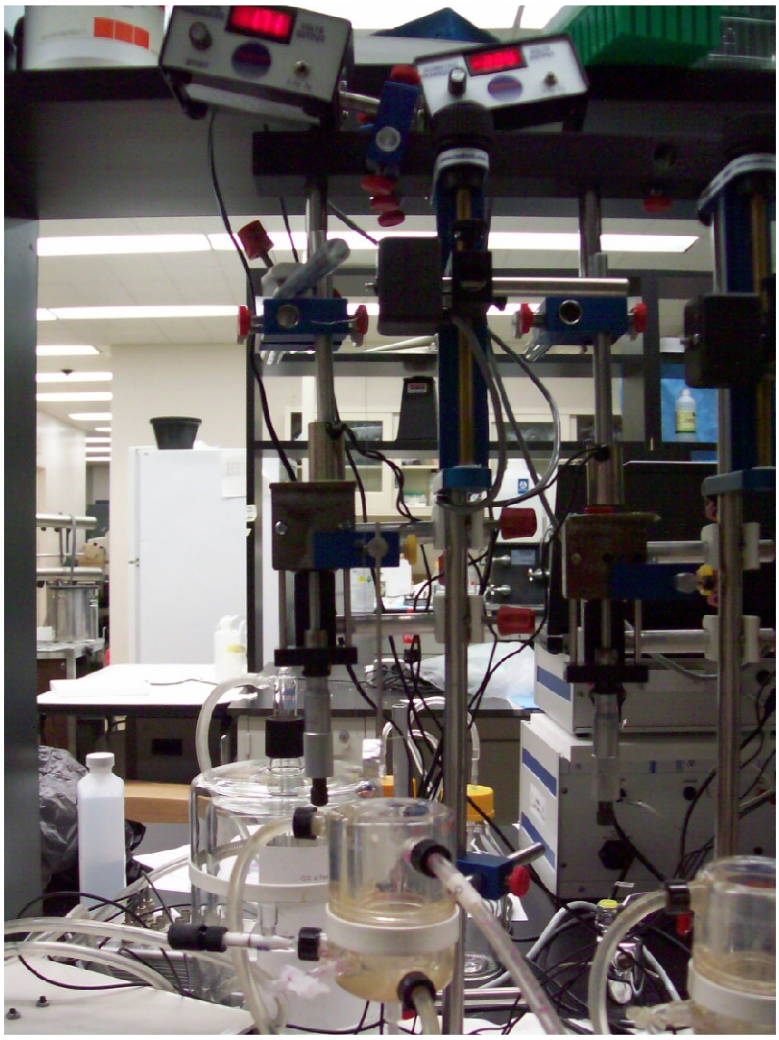

Figure 2.5 The mechanical testing apparatus.

Each tissue ring was looped over a wire hook connected to an isometric force transducer (model 52-9545, Harvard Apparatus, South Natick, MA) and a lower horizontal bar connected to sliding element. The horizontal bar was held in place by a steel plate controlled by an electro-magnetic hold/release system. When the electro-magnetic control was on, the steel plate was fixed such that the lower horizontal bar remained a set distance from the wire hook of the force transducer. This "zero-stretch" distance, termed here L_o, was initially manually adjusted upon first attaching the tissue

ring onto the system. This manual adjustment was made by turning a knob connected to the isometric force transducer wire hook, and could be reliably set in 0.5 mm increments. The electromagnet could be switched off using a button control. Once triggered, the steel plate holding the horizontal bar suddenly fell by a pre-adjusted length. The lower bar remained at this new length, continually stretching the tissue ring. This stretch length, ΔL, was controlled by a micrometer, which was set when the electromagnet was on, and could be controlled to the nearest micrometer. After the force response was sufficiently recorded, the steel plate was manually raised so that it was re-attracted to the magnet, returning the horizontal bar to original L_o length.

The mechanical apparatus could then be used for repetitive stress-relaxation testing. In each cycle, the button control suddenly lowered the magnetic plate to produce and maintain a stretch. At the end of the test, the magnetic plate was manually raised to return the tissue to its original length, L_o.

Throughout the duration of the mechanical testing, the force response was output from the force transducer to a computer running the data acquisition system Notocord® (NOTOCORD Systems SAS, Croissy-sur-Seine, France). Preliminary force response recordings without any loaded biological sample showed that a considerable high frequency component (about 100 Hz) and low frequency component (about 4 Hz) were extraneously produced in the force signals. It was assumed that these artifacts were associated with (1) the impact from the sudden drop of the steel plate, and (2) the swinging of the wire hook, respectively, and were unavoidable in this experimental setup. In order to cope with this noise, a sampling rate of 500 Hz was chosen (which is

sufficiently high to avoid aliasing for force signals up to 250 Hz), with the hope of later digitally filtering the signal to remove the noise.

2.2.1 Calibration of Force

The force transducer was calibrated while running the Notocord® data acquisition system. The force transducer had 2 force settings- "5g" or "0.5g" with which to apply the maximum voltage output of 5V. Results from previous works (Wakatsuki et al., 2000) suggested that the maximum force would be substantially less than 1 g. Thus, the "0.5g" setting was chosen with which to apply the maximum voltage output of 5V. Additionally, before each series of testing the force transducer was calibrated in Notocord® using recordings obtained from hanging a 120 mg standard weight on the wire hook of the force transducer.

2.2.2 Choice of Stretching Parameters

The choices of appropriate values for the initial length L_o, and the stretch amount ΔL, were crucial parameters in this experimental design. Since the objective was to measure the cellular response, a small strain was optimal. This can be reasoned from a hypothetical stress-strain relationship graph of the loading of cellularized tissue. It was expected that collagen would become more exponentially stiff than the other components in living reconstituted tissue at higher strains. Thus, since the collagen response dominates at higher strains, a small strain level should be chosen to best capture the cellular response from the tissue rings. For these experiments, an upper limit of 10% strain was decided upon.

The choice of the initial length L_o was chosen after trial and error. Ideally, this length should be the natural unloaded length of the ring. However, in practice, this length is difficult to gauge during experimentation. For instance, the real-time recorded output from the force transducer showed too much noise to accurately determine this "zero force" baseline for each tissue ring without prior digital filtering. An alternate approach was to choose a predefined L_o value to be used for all experiments. Since all tissue rings were formed around mandrels having the same fixed circumference, there was in fact already a fixed standard length to the tissue rings that was implicit in the experimental protocol.

Initial choices for this length came from approximations of the tissue length while around the mandrel, as used in previous studies (Nagendra, 2010). Since the mandrel around which the tissue ring was molded has a 14.1 mm circumference, an approximate resting length is about half of that value, 7 mm. An initial value of L_o was chosen by halving this value to 3.5 mm. This conservative estimate was initially selected so as to not risk breaking the tissue rings during experimentation. However, the results from preliminary experimentation showed insignificant amounts of force were recorded from stretching with this low value for L_o and a 10% strain (ΔL of 0.35 mm).

The plausibility of using a larger value of L_o was investigated. Stretches using a value of 5 mm yielded variable results, with some rings still producing negligible forces from a 10% strain. A still larger value was sought. Speculating that the tissue rings were under considerably less circumferential compression while forming around the mandrel than had previously been assumed, an approximation of the natural length was made by measuring the length of the flattened tissue ring while off the mandrel and inside a tissue

culture dish using calipers, as described above. In fact, in preliminary experiments this length was found to range from 7 to 9 mm. An L_o of 10 mm was chosen, as it was assumed to be greater than even the tissue ring with the greatest unloaded length. Additionally, a stretch, or ΔL, of 1 mm was selected for ease of setting the strain micrometer during experimentation, and because it constituted a small strain (10%).

2.3 Experimental Procedure

After the tissue ring was looped around the wire hook and horizontal bar of the mechanical testing apparatus, it was lowered into a thermo-regulated organ bath (Harvard Apparatus, South Natick, MA), which was kept at 37°C, containing 50 mL of DMEM. The tissue ring was pre-conditioned by slowly (over a span of 30 seconds) using the strain micrometer to increase the separation between the wire hook and horizontal bar from about 0 to 11 mm, and subsequently return the horizontal bar to its initial position over the span of 60 seconds. After waiting 120 s, the mechanical apparatus was adjusted to the standard L_0 (= 10.00 mm) and ΔL (= 1.00 mm) parameters chosen.

After another period of 120 s, the tissue ring was stretched three times. The force response during each stretch was recorded for 120 s, and was followed by a recovery period of 120 s between stretches. Preliminary experimentation showed that the first stretch produced a much larger force response than subsequent stretches. Additionally, the forces recorded from the second and third stretches were observed to be of similar magnitude, indicating that the stretches were reasonably reproducible.

2.4 Determining the Cellular Contribution

The cellular contribution was determined by treating the tissue rings with cytochalasin-D (CD) to disrupt the actin cytoskeleton of the VSMCs. This completely eliminated the force contribution of VSMCs to the tissue stiffness, and left only the collagen ECM to generate the resulting tissue stiffness, termed here the passive stiffness. The cellular contribution to the tissue stiffness, or active stiffness, could be estimated from the relative difference of the intact tissue and passive stiffnesses. After adding CD (dissolved in DMSO) to the DMEM-filled organ bath (to a final concentration of 2 μM) and waiting 500 s for diffusion through the tissue, the tissue ring was given a final stretch. The force response was recorded, as described before. A schematic of the entire experimental mechanical protocol is shown on the next page in Figure 2.6.

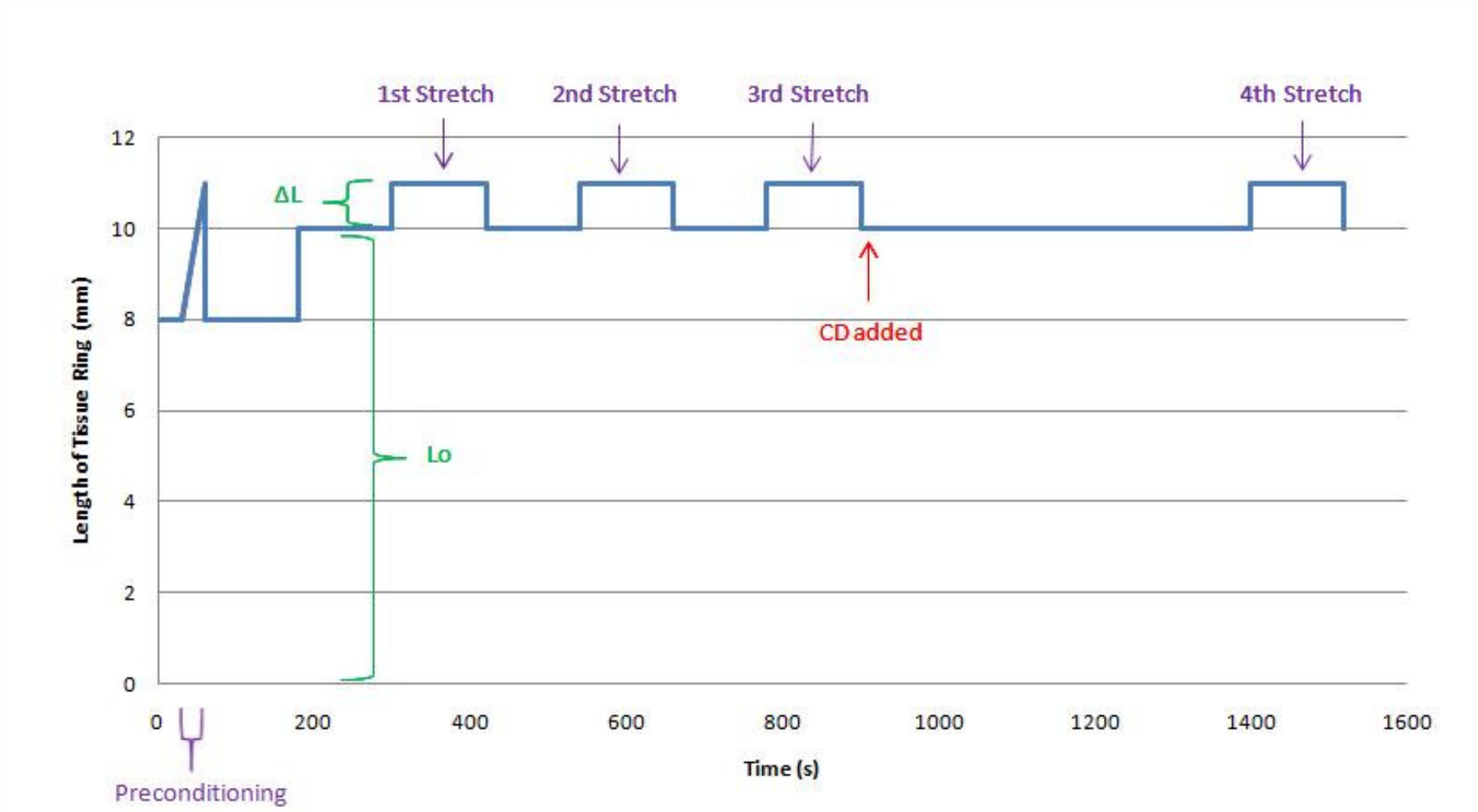

Figure 2.6 A schematic of the experimental mechanical procedure. Note that the length of the unloaded tissue ring was found to vary between 7-9 mm, so there may have been some variability in this length before and after preconditioning. CD = cytochalasin D, which was added to disrupt the actin filaments in the cytoskeleton.

2.5 Digital Filtering and Analysis of the Output Signal

The force recording during each stretch was separately exported from Notocord® into text files ('.txt'), which was imported into MATLAB (version 7.10.0) for digital filtering and analysis. A digital filter was needed to remove noise recorded in the force signal, as was mentioned above. Since a relatively lower frequency force response was anticipated from the tissue rings (about 1-2 Hz), a low pass filter was sought to remove the higher frequency noise in the signal. A Butterworth low pass filter was chosen for its property of maximally flatness (a gain magnitude close to 1) over the range of desired frequencies, as shown in Figure 2.7.

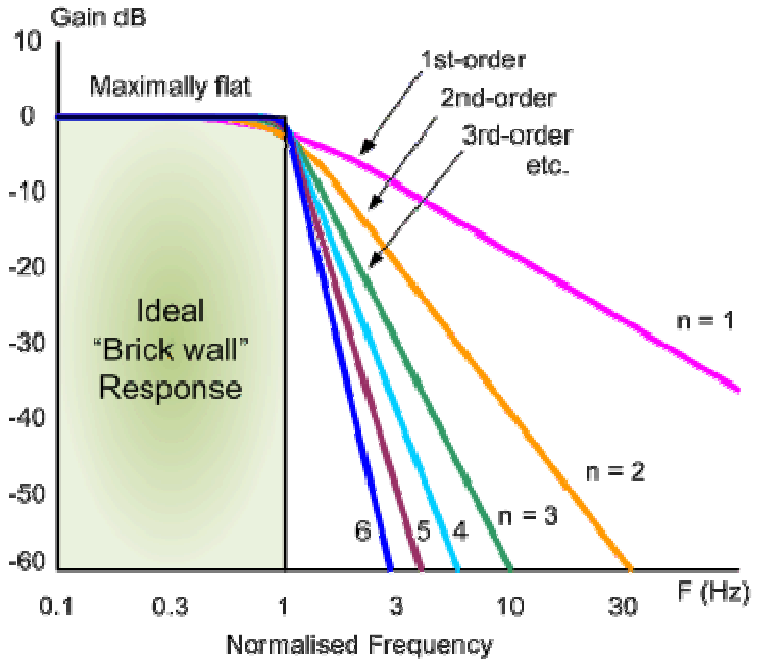

Figure 2.7 Gain versus frequency of a low pass Butterworth filter.
Source: (Storr, 2011)

Computation of the coefficients of the Butterworth filer and the filtering itself were done using the MATLAB commands ‘butter’ and ‘filtfilt’ (see Appendix A), respectively. The order and cutoff frequency parameters for the filter were chosen by trial and error. The parameters producing the smoothest force decay while minimizing the loss in initial peak force were chosen. Eventually, a filter order of 4 and cutoff frequency of 4 Hz were selected. An example of the effect of the digital filtering on a segment of data is shown in Figure 2.8.

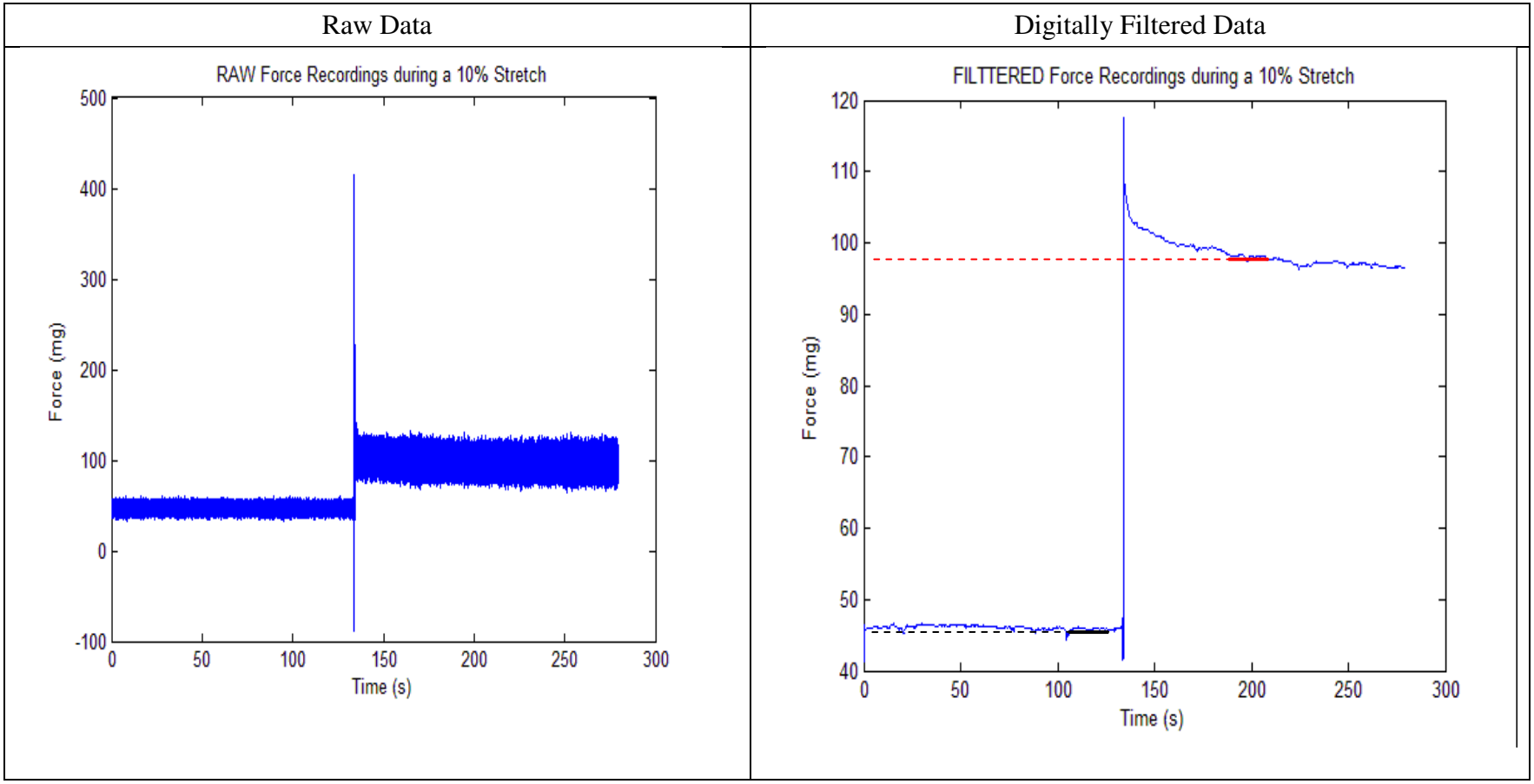

Figure 2.8 The effect of digitally filtering the raw data. Plots of the raw and filtered (fourth-order low pass Butterworth with a cutoff frequency of 4 Hz) force recordings from a single stretch are compared. Approximate baseline (black) and steady-state (red) levels are indicated with dashed lines; the averaged force values used for computation are shown with solid lines.

The filtered output of the force response over time and the tissue dimensions were used to estimate the change in stress incurred from stretching each tissue ring. The engineering stress was calculated by dividing the net change in force produced from the stretch by the initial cross-sectional area of the ring. The net change in force was determined in MATLAB by subtracting averaged values of baseline and steady-state forces recorded from the stretch (Appendix A). These averaged baseline and steady-state force values were consistently found for each stretch for all tissue rings by averaging the force 5-25 seconds before and 90-110 seconds after the largest force recorded (Figure 2.8). The cross-sectional area was computed from twice the product of the thickness and the width off of the mandrel.

These computed changes in stress were used to calculate three elastic moduli of the tissue rings. First, the total tissue elastic modulus was found from the quotient of the change in stress due to the third stretch and the change in strain, which was 0.10 for all stretches. Second, the matrix elastic modulus due to the ECM only was found by dividing the difference in the changes in stress from the third and fourth stretches (after adding CD) by the strain. Finally, an estimate of the cellular elastic modulus was determined from the difference between the total tissue and matrix elastic moduli.

2.6 Statistical Analysis

Comparisons of the recorded dimensional data and computed elastic moduli of each tissue ring were made amongst the four groups (5 weeks/18 weeks, WKY/SHR). The statistical significance of the differences in the reported values was determined from two-way ANOVA testing. A p value of less than 0.05 was considered significant.

CHAPTER 3

RESULTS

The VSMCs from four individual rats were used, one for each strain-age combination. The cells from each individual rat were expanded in number, to produce seven rings that were individually tested (so n = 7 for each statistical group). ANOVA testing was used to determine the statistical significance for each group ($p < 0.05$).

3.1 Comparisons of Tissue Dimensions

The tissue thickness, width, and length, as referenced on the mandrel, unloaded state, and while looped on the force transducer, referenced in the following sections are illustrated in Figures 3.1 to 3.3.

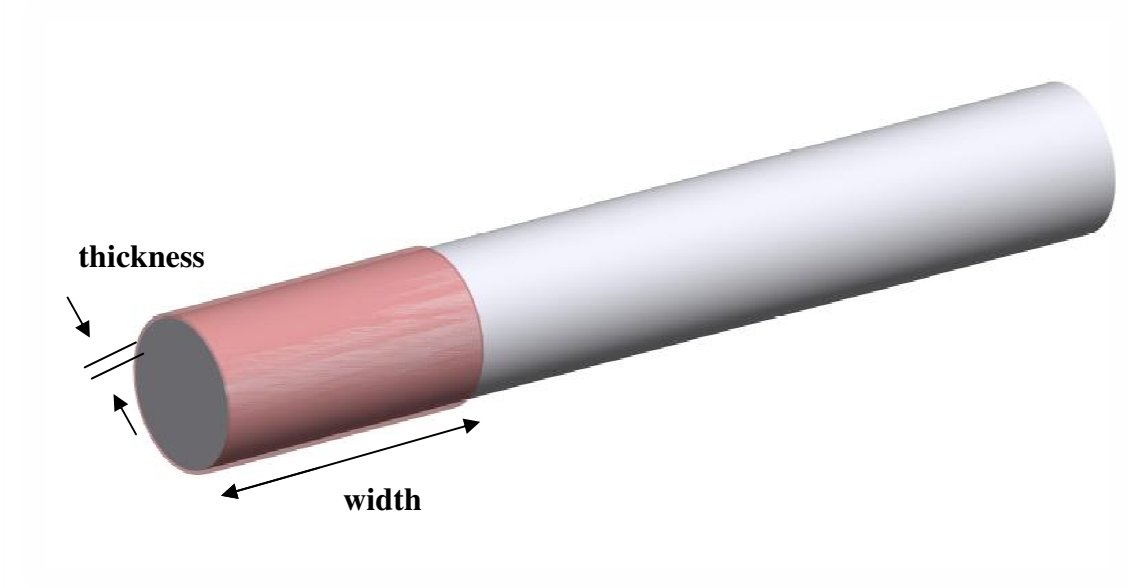

Figure 3.1 Illustration of width (axial extent) and thickness of the tissue ring on the mandrel.

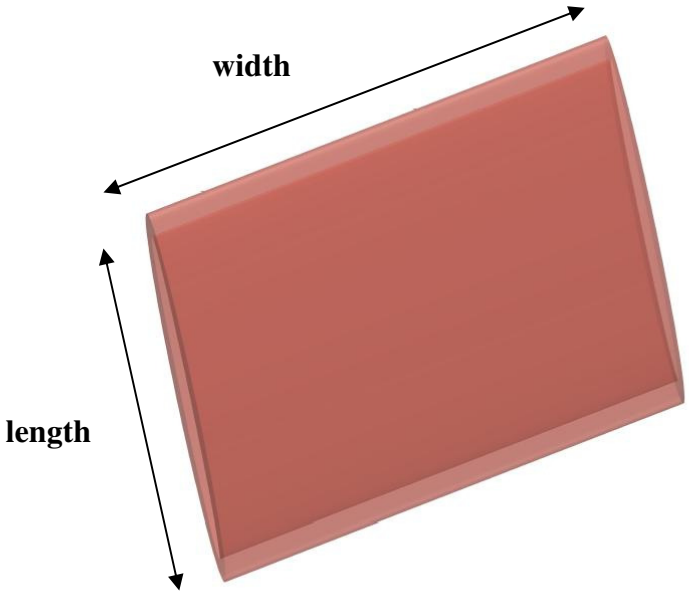

Figure 3.2 Illustration of the unloaded, flattened tissue ring's width and length. Note: the culture dish not shown.

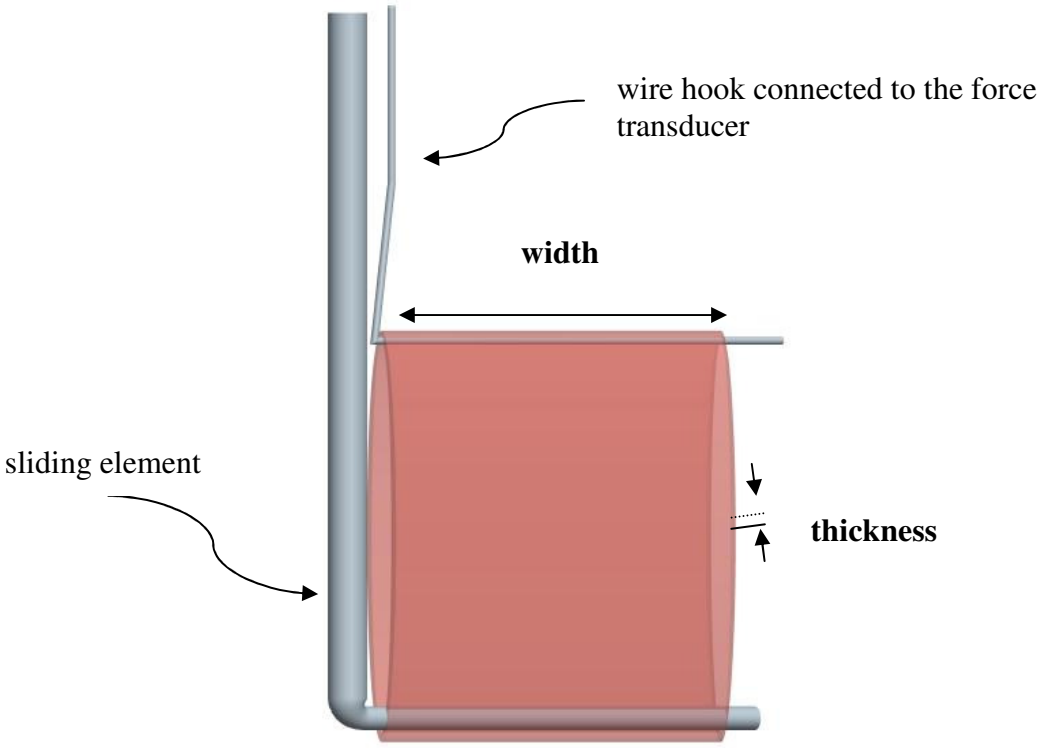

Figure 3.3 Illustration of the tissue ring looped around the wire hook of the force transducer and sliding element. Twice the product of the width and thickness determined the cross-sectional area.

3.1.1 Tissue Thickness

The tissue thickness was measured through images of the circular cross-sectional area of the tissue ring while on the mandrel, and visually determined using the MATLAB Image Processing Toolbox. Preliminary experiments showed that this relatively small value did not vary much across tissue rings in the same experimental group or even between groups. The average tissue thickness was found to be 43.9 ± 5.0 (mean ± SD) pixels. From images of a length standard, it was determined that 280 pixels ≡ 1.00 mm. Thus, a thickness measure of 0.157 mm was assumed for all tissue rings. It is interesting to note

that this represents an almost 8-fold decrease from the assumed pre-incubation tissue thickness, which was the space between the outer and inner diameter, 1.25 mm.

3.1.2 Axial Extension Ratios during Incubation

A comparison was made of the tissue widths along the mandrel before and after incubation. The tissue width before incubation was assumed to be the same for all samples, because the same volume of VSMC-collagen gel was used to construct each ring. This initial width along the mandrel was equal to the height of gel solution in the cylindrical mold, which was determined by dividing the total volume (200 μL = 200 mm^3) by the annulus area of the mold (annulus area = π[(inner radius of cylindrical tube)^2 – (radius of mandrel)^2] = $\pi[3.5^2 - 2.25^2]$ = 22.58 mm^2). This yielded a pre-incubation width along the mandrel of 8.86 mm.

The measured widths on the mandrel after incubation were noted to be larger than this pre-incubation value. However, no measurement of the width along the mandrel could be taken for any of the tissues containing the 18-week old SHR VSMCs. It was discovered after disassembling the cylindrical mold that these tissues slipped down the mandrel during the incubation process, whereby they did not adhere to the axis of the mandrel to any significant degree.

To get a sense of how incubation along the mandrel affected this axial dimension of the tissue rings that remained attached, the measured tissue width on the mandrel of each ring was normalized to the pre-incubation value (8.86 mm) to produce a mandrel incubation axial extension ratio. The mean ± SEM ratios for these strain-age combinations are shown in Figure 3.4. In this case, a one-way ANOVA test was used to determine the statistical significance among these groups ($p < 0.05$).

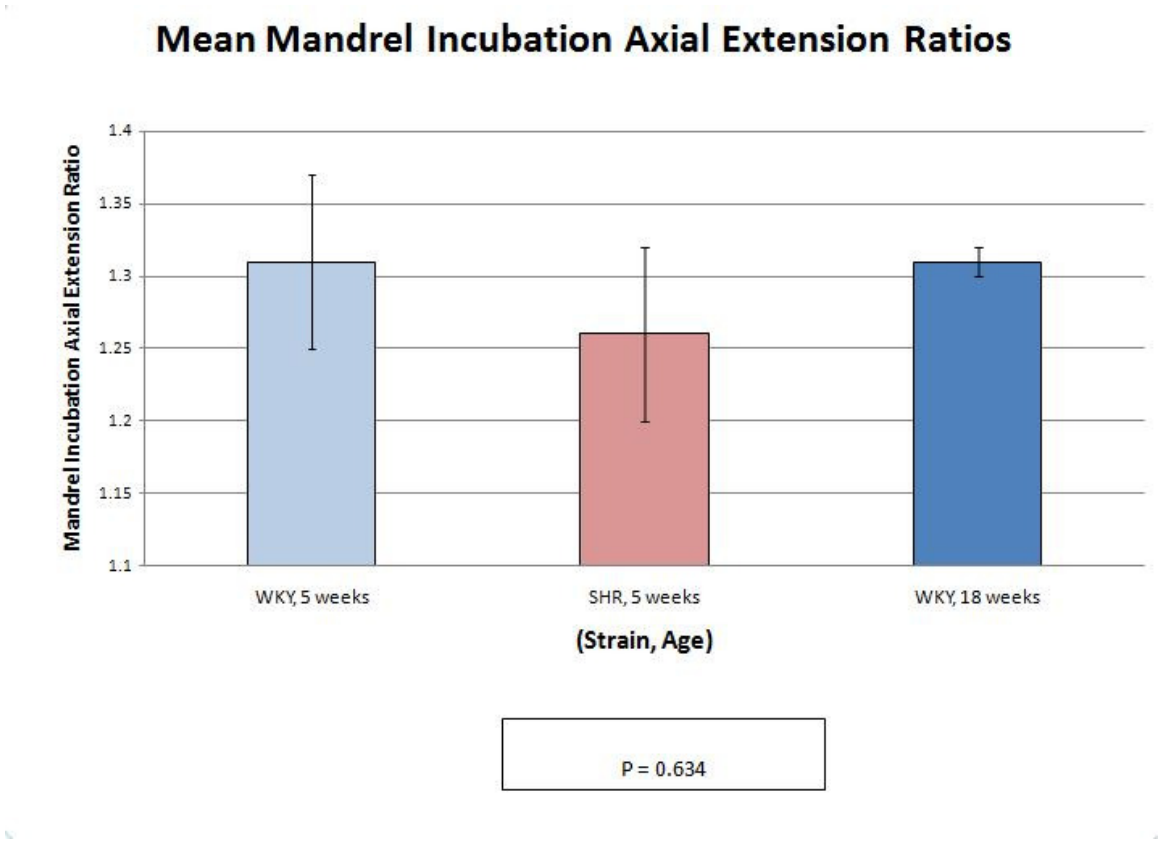

Figure 3.4 Mean ± SEM mandrel incubation axial extension ratios of post- and pre-incubation tissue widths along the axis of the mandrel. The mandrel incubation axial extension ratio is a ratio of the tissue width along the mandrel after incubation on the mandrel for two days compared to the gel extent on the mandrel immediately after being loaded into the tissue mold. Note: no value for tissues containing 18-week old SHR VSMCs could be determined because these tissues slipped off of the mandrel during incubation.

No statistical significance was found in these mean axial extension ratios ($p = 0.634$) amongst the strain-age combinations tested.

3.1.3 Unloaded Widths

After the tissue ring was removed from the mandrel to a culture dish, it flattened into a double sheet-like structure. Importantly, these unloaded widths were used in the calculation of the cross-sectional area to determine the engineering stress produced on the rings from each stress. The width of the each ring was measured using calipers. For all

but one tissue ring (which, contained 18-week SHR VSMCs), this unloaded tissue width was greater than the initial pre-incubation width (8.86 mm). This indicates that, in general, VSMCs remodeled the collagen through axial extension. This extension is distinct from that existing on the mandrel. A comparison of the mean ± SEM of this unloaded width dimension is shown for each strain-age combination in Figure 3.5.

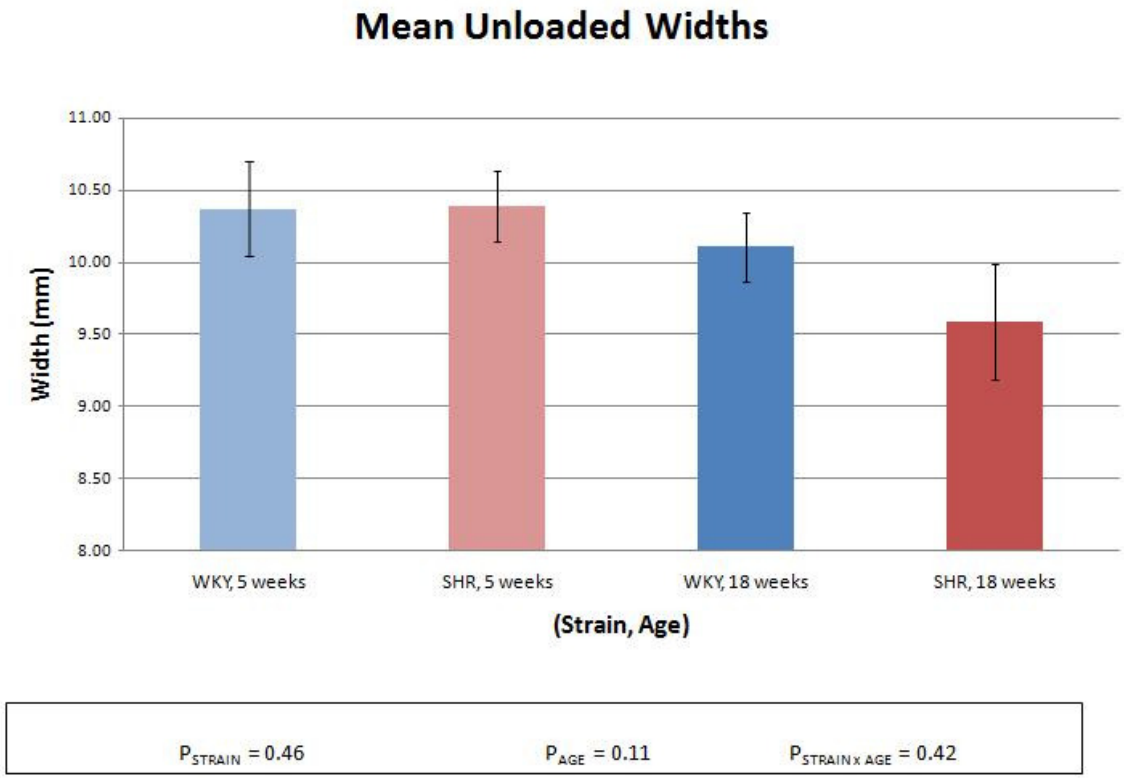

Figure 3.5 Mean ± SEM unloaded widths of the tissue rings for each strain-age combination.

A two-way ANOVA test showed no significant differences in the mean unloaded widths found for stain, age, or their interaction.

3.1.4 Unloaded Axial Width Ratios

After removal from the mandrel, the tissue rings were observed to decrease in width. This implies that the ring was extended on the mandrel compared to its width when the interaction with the mandrel was removed. A measure of this increase in width due to interaction with the mandrel was made by normalizing the measure of width on the mandrel to that measured off of the mandrel. The mean ± SEM values for each strain-age combination for this unloaded axial width ratio are shown in Figure 3.6. Note that this could not be done for the tissues containing the 18-week old SHR VSMCs because no measure of the width on the mandrel could be taken, as explained above.

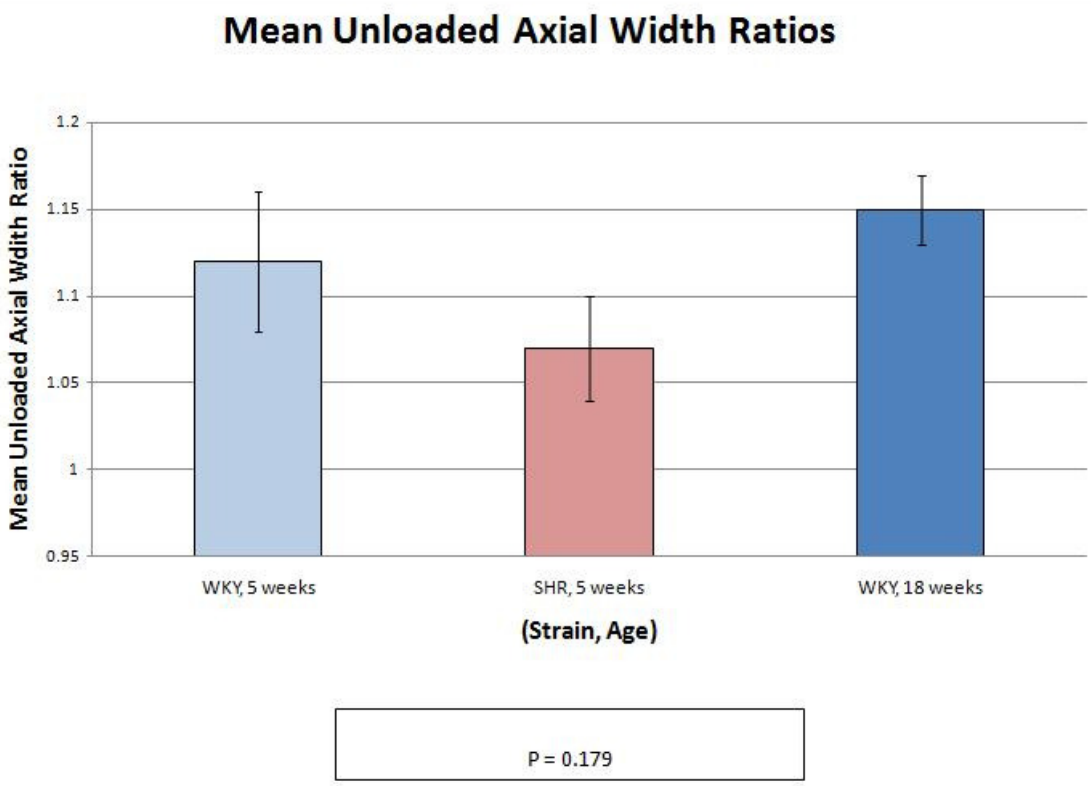

Figure 3.6 Mean ± SEM unloaded axial width ratios. The unloaded axial width ratio is a ratio of the tissue width along the mandrel after incubation compared to the unloaded width of the tissue ring. Note: no value for tissues containing 18-week old SHR VSMCs could be determined because these tissues slipped off of the mandrel during incubation.

Here, a one-way ANOVA test shows no statistical significance between the strain-age combinations tested.

3.1.5 Unloaded Tissue Lengths

Similar to the unloaded tissue width, the length of the flattened out unloaded tissue was measured. Each tissue ring had a larger length than half of the circumference of the mandrel, indicating that the tissue rings' interaction with the mandrel had acted to

circumferentially compress the tissue. A comparison of the mean ± SEM of this dimension is shown for each strain-age combination in Figure 3.7. Note that if there had been no mandrel to compress the ring around it, the length of the rings would have been 7.07 mm (i.e., half of the 14.14 mm circumference of the mandrel).

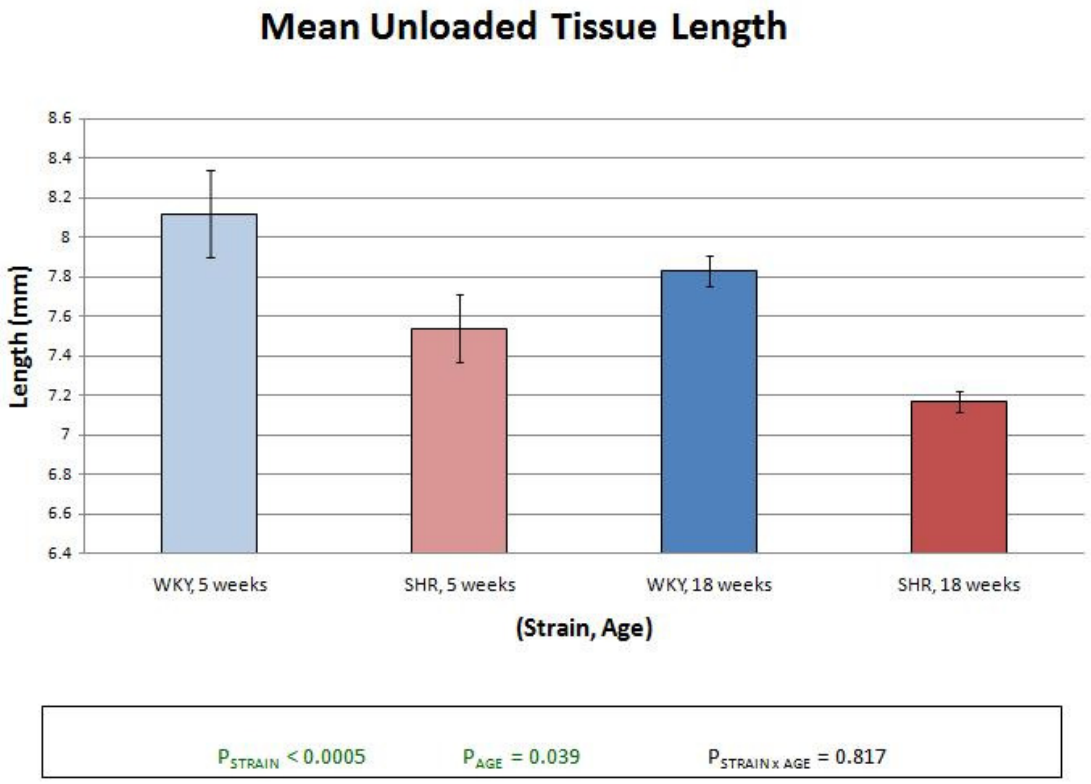

Figure 3.7 Mean ± SEM unloaded tissue length for each strain-age combination.

The results of a two-way ANOVA test indicate that the unloaded tissue length is decreased with hypertensive strain ($p < 0.0005$) and older age ($p = 0.039$). Since the interaction term was not significant ($p = 0.817$), these effects are independent.

3.2 Force Recordings

The force response of the tissue rings were recorded during the stretches using the NOTOCORD data acquisition software, described previously. These raw force signals were digitally filtered (fourth order low pass Butterworth filter with a cutoff frequency of 4 Hz) to remove higher frequency noise from the signal. Figures 3.8 to 3.11 show typical examples of these filtered force recordings for each strain-age combination of tissue ring. A comparative look at these signals is shown in Figure 3.12.

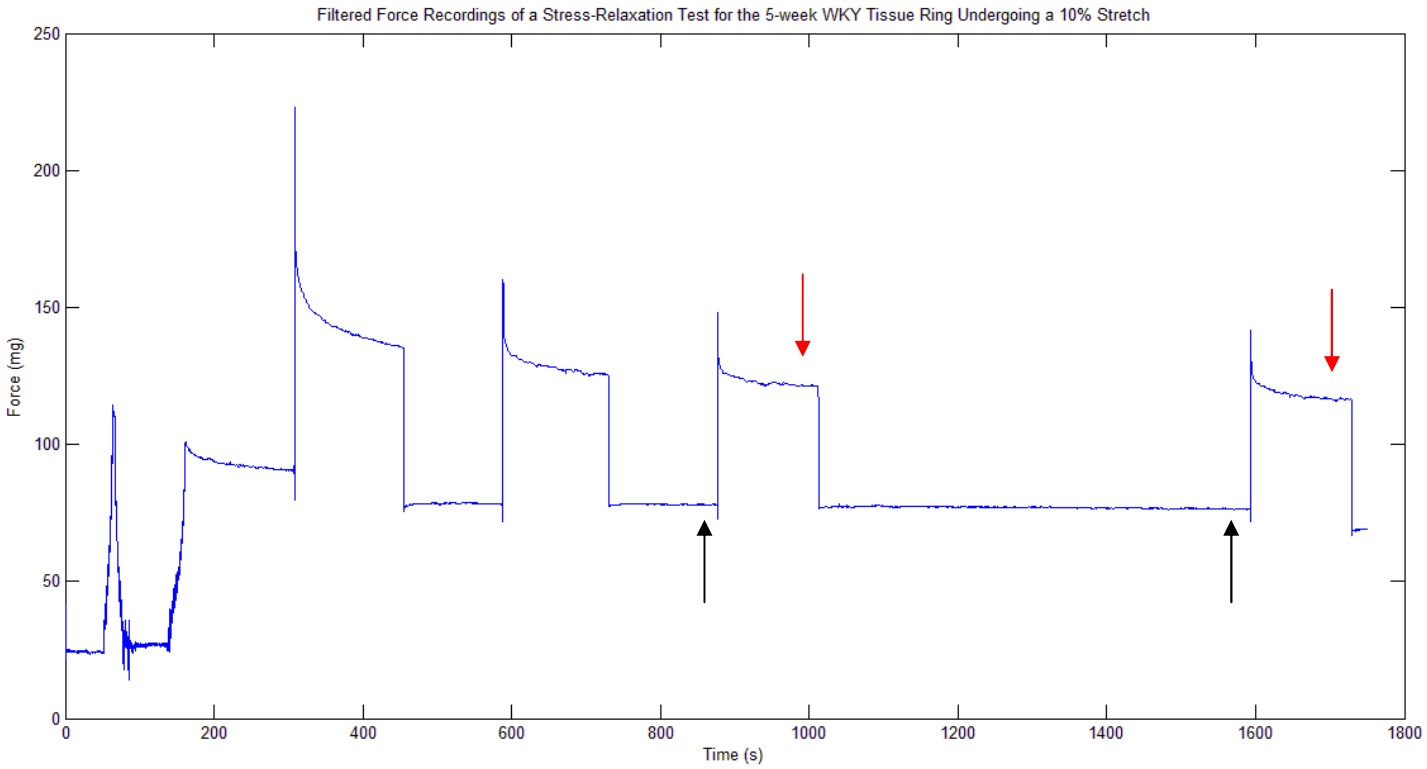

Figure 3.8 Example filtered force response over time from a tissue ring containing 5-week old WKY VSMCs. Approximate points used for baseline (black) and steady-state (red) are shown with arrows. The first set of arrows corresponds to values used to compute the total tissue elastic modulus, while the second set refers to that used for the matrix elastic modulus.

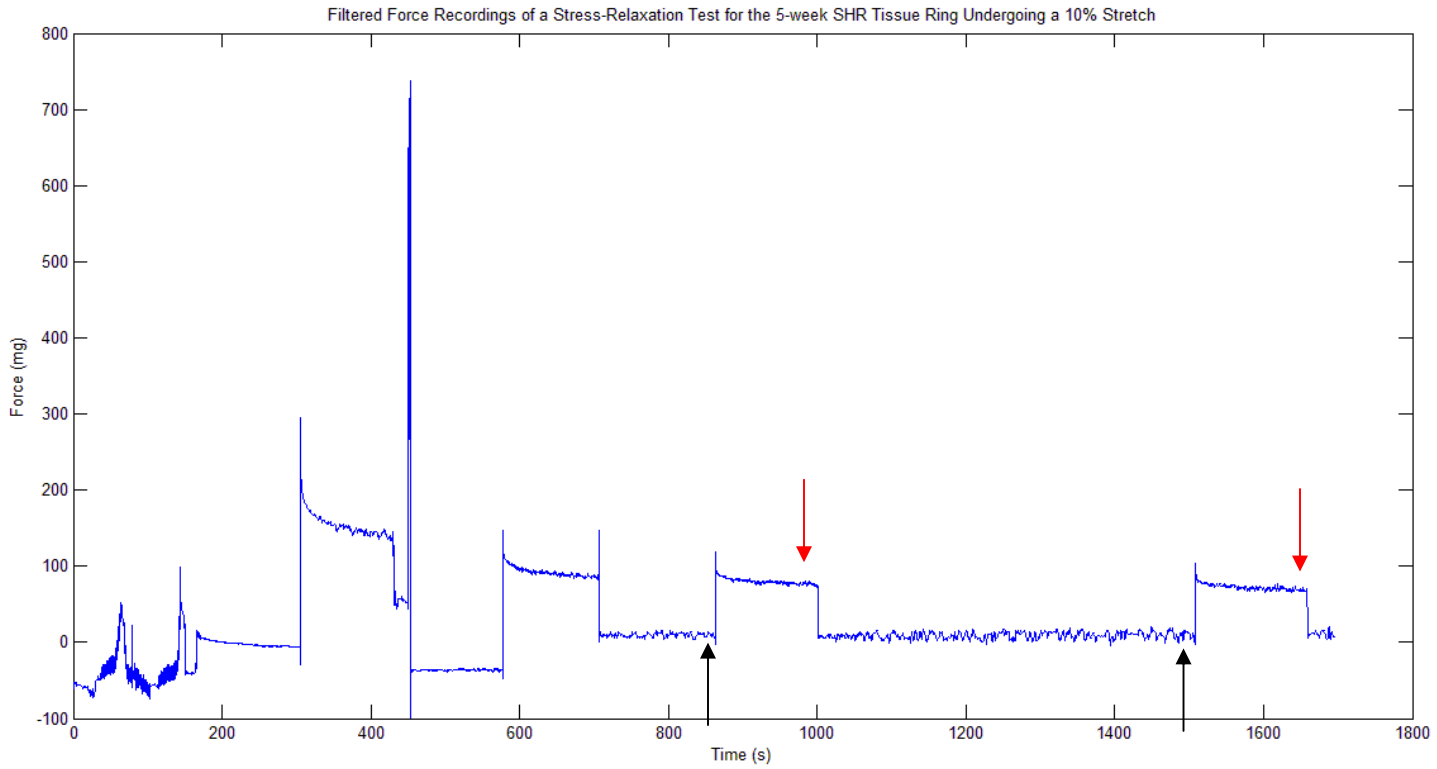

Figure 3.9 Example filtered force response over time of a tissue ring containing 5-week old SHR VSMCs. Approximate points used for baseline (black) and steady-state (red) are shown with arrows. The first set of arrows corresponds to values used to compute the total tissue elastic modulus, while the second set refers to that used for the matrix elastic modulus.

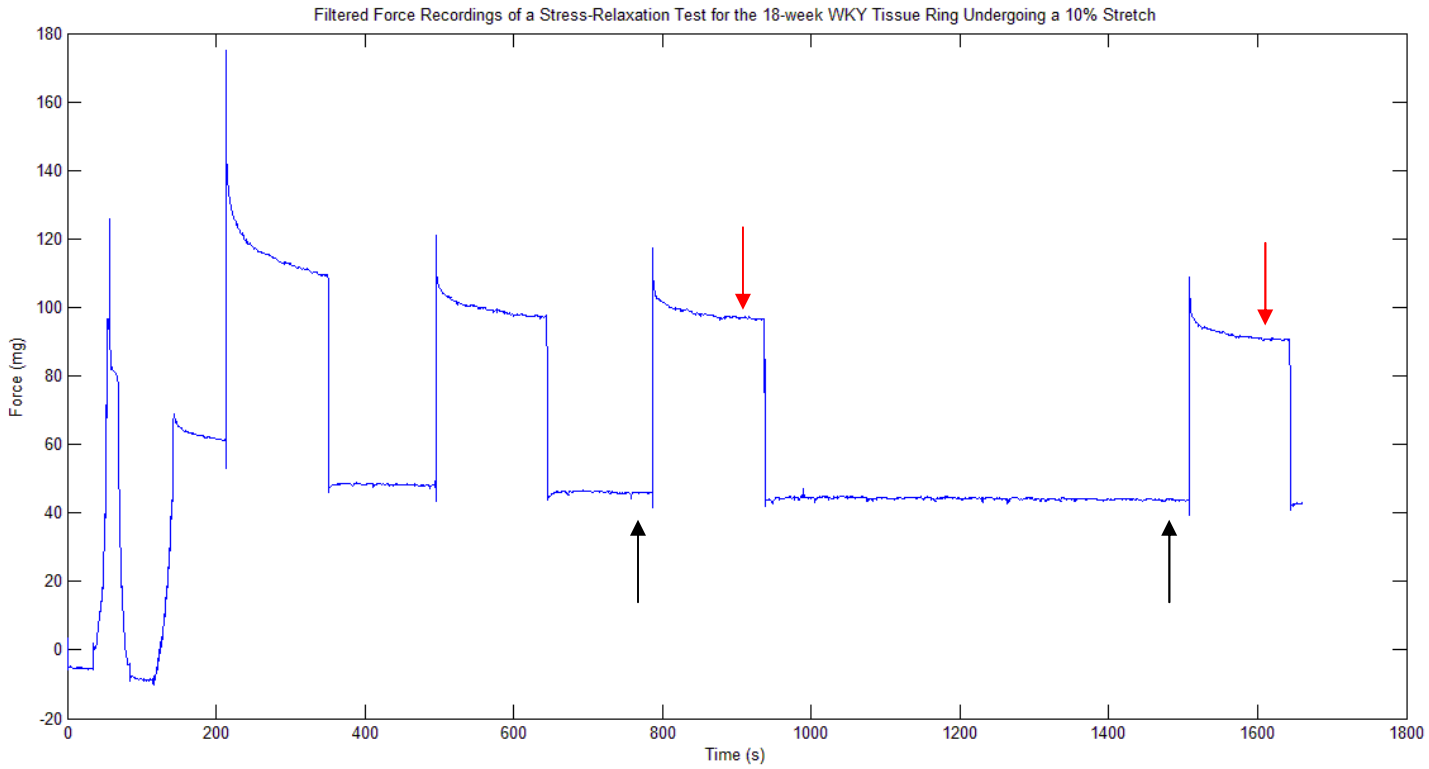

Figure 3.10 Example filtered force response over time of a tissue ring containing 18-week old WKY VSMCs. Approximate points used for baseline (black) and steady-state (red) are shown with arrows. The first set of arrows corresponds to values used to compute the total tissue elastic modulus, while the second set refers to that used for the matrix elastic modulus.

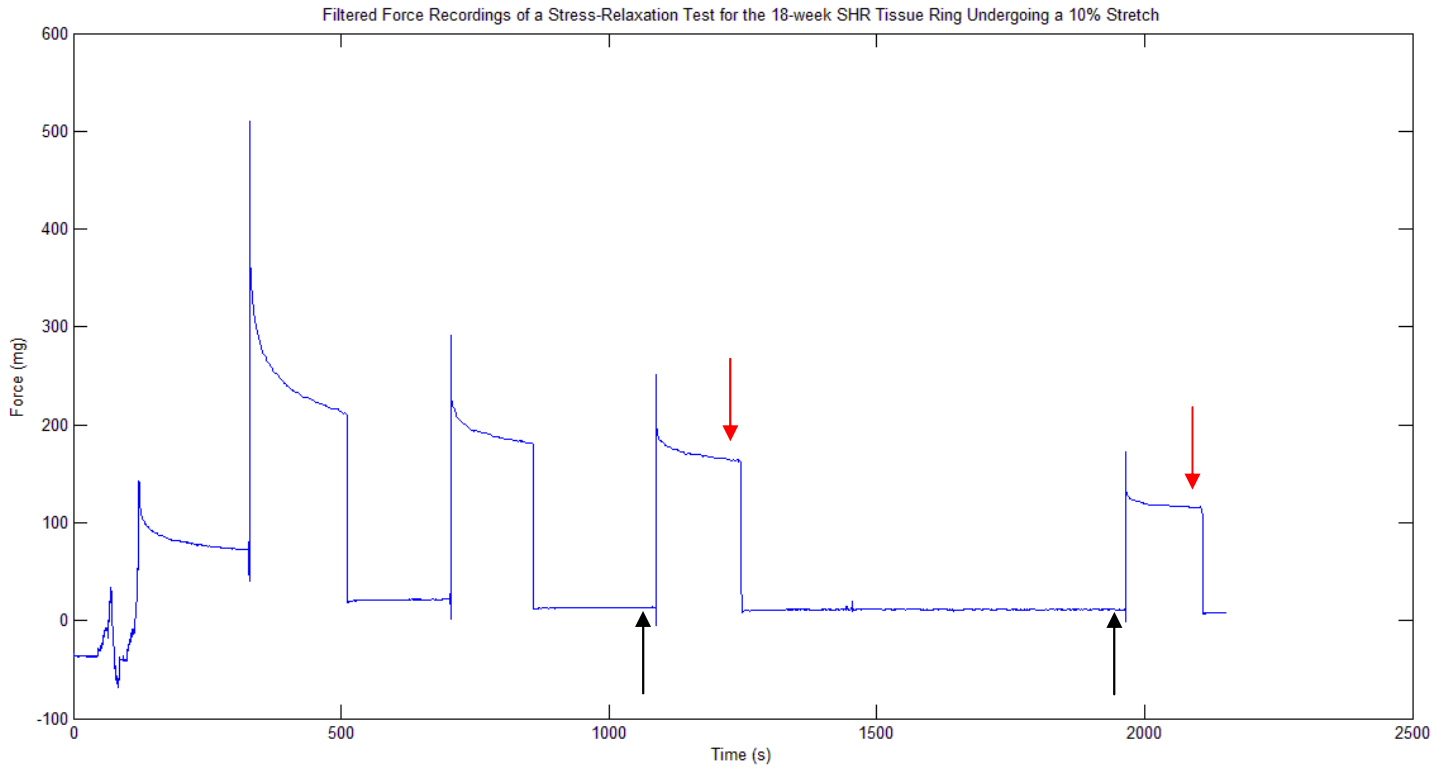

Figure 3.11 Example filtered force response over time of a tissue ring containing 18-week old SHR VSMCs. Approximate points used for baseline (black) and steady-state (red) are shown with arrows. The first set of arrows corresponds to values used to compute the total tissue elastic modulus, while the second set refers to that used for the matrix elastic modulus.

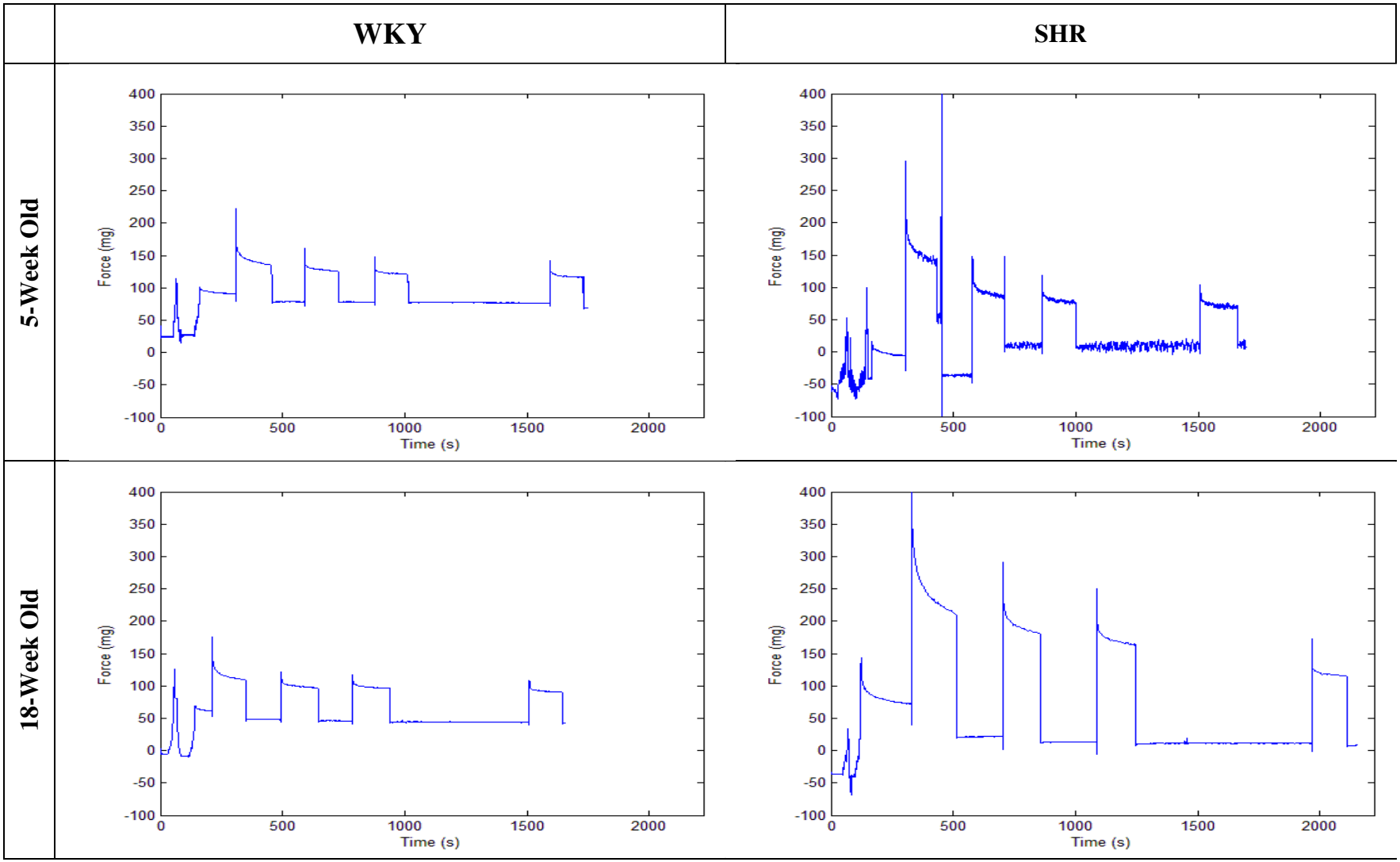

Figure 3.12 A comparison of example filtered force responses over time from tissue rings for each strain-age combination. Note the scales of the graphs have been adjusted to be the same.

3.3 Calculated Tissue Elastic Moduli

Tissue elastic moduli were determined from the quotient of the computed engineering stress and the 10% strain. The engineering stress was determined from the difference in steady-state and baseline forces divided by the cross-sectional area at the baseline state.

The cross-sectional area at the baseline state could not be reasonably measured, so two methods to approximate this area were utilized. In the first method, the baseline cross-sectional area is determined from the approximate dimensions of the tissue ring in both the unloaded state and while on the mandrel. The cross-sectional area is computed from twice the product of the width (measured in the unloaded state) and the thickness (measured while on the mandrel). In this case, two assumptions are made: the unloaded width of the tissue ring on the mandrel does not significantly change to produce the baseline width, and the tissue thickness does not significantly change in any state (on the mandrel, unloaded, and on the mechanical testing apparatus).

In the second method, the cross-sectional area at the baseline state is approximated from the dimensions of the tissue ring while on the mandrel only. Twice the product of these dimensions produces the cross-sectional area while on the mandrel. Along with the L_0 (10.00 mm) used in the baseline state, and the assumption of tissue incompressibility, the cross-sectional area on the mandrel can be used to approximate the cross-sectional area at the baseline state.

Of course, this second method can only be used for those tissue rings that remained adhered to the mandrel during the full incubation period. Thus, this second method cannot be used for the tissue rings containing the 18-week SHR VSMCs. To cope with this limitation, the first method of estimating the cross-sectional area is initially

used to compute the tissue elastic moduli. The tissue moduli, except for the 18-week SHR, are then recalculated using the cross-sectional areas derived from the alternative, second method.

3.3.1 Total Tissue Elastic Moduli

The total tissue elastic modulus for each tissue ring was computed using the net force difference produced by the third stretch, when the force response was reasonably repeatable. The mean ± SEM total tissue elastic moduli is shown in Figure 3.13 for each strain-age combination.

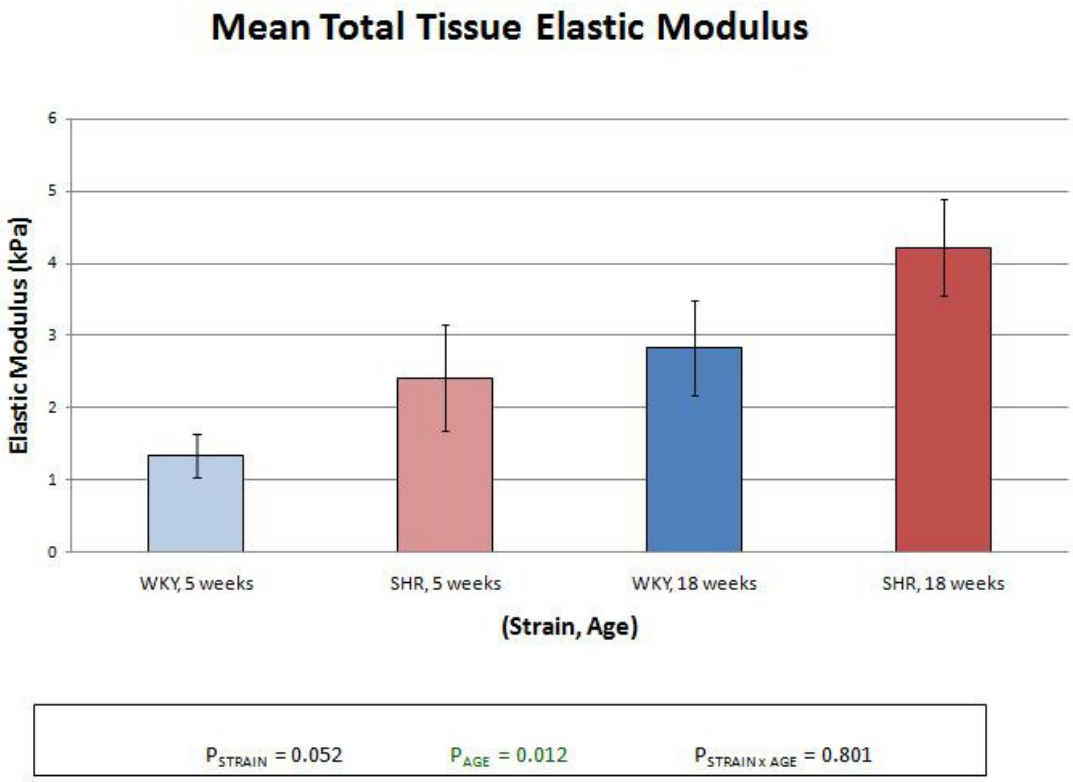

Figure 3.13 Mean ± SEM total tissue elastic modulus for each strain-age combination.

Results from a two-way ANOVA test showed a greater total tissue stiffness with older age for each strain ($p = 0.012$), and an almost significantly greater total tissue stiffness in SHR for each age ($p = 0.052$). Since the interaction term was not found to be significant ($p = 0.801$), these factors, strain and age, independently affect the total tissue elastic moduli.

3.3.2 Extracellular Matrix Elastic Moduli

The elastic moduli of the extracellular matrix were computed using the net force of the fourth stretch, after the tissue had been treated with cytochalasin D, which effectively eliminated the VSMCs force exerting capability (through the actin cytoskeleton). Thus, the resulting collagen matrix was the only contributor to force. A comparison of the mean ± SEM of the matrix elastic moduli is shown in Figure 3.14 for each strain-age combination.

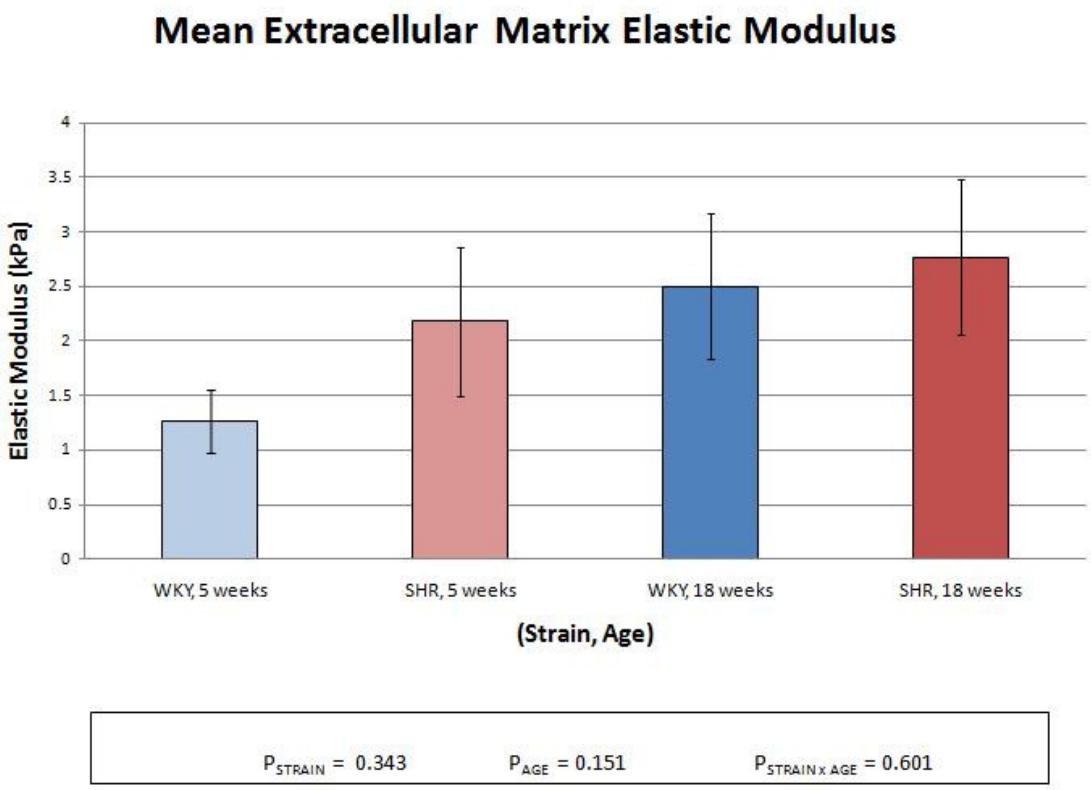

Figure 3.14 Mean ± SEM extracellular elastic moduli for each strain-age combination.

No statistical significance was found between extracellular matrix elastic modulus amongst each strain-age combination.

3.3.3 Cellular Elastic Moduli

The cellular elastic modulus, the contribution of the VSMCs, was estimated from the difference between the total tissue and matrix elastic moduli for each tissue ring. The mean ± SEM of the cellular elastic modulus is shown in Figure 3.15 for each strain-age combination.

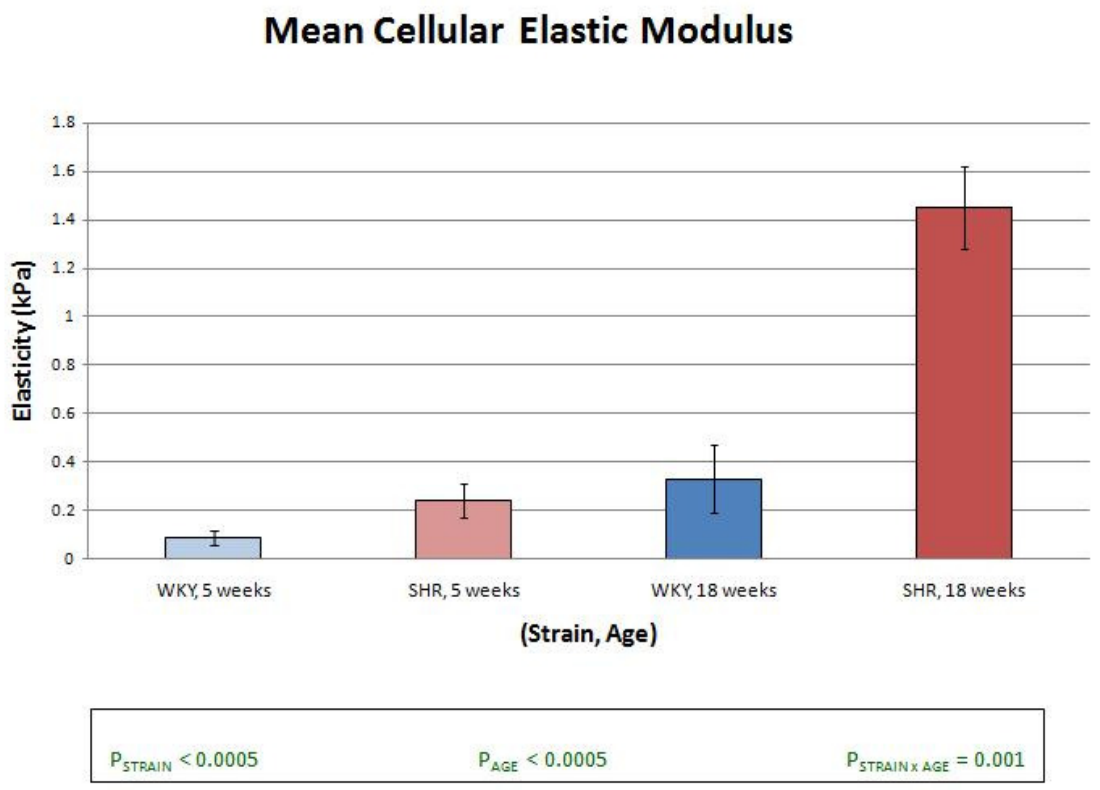

Figure 3.15 Mean ± SEM cellular elastic modulus for each strain-age combination.

By two-way ANOVA testing, both factors, strain and age, were both found to increase the cellular elastic modulus ($p < 0.0005$ for each factor). Moreover, the interaction between the two was found to be highly significant ($p = 0.001$).

Older age produced a greater than a 6-fold difference in the cellular elastic moduli estimated for SHR VSMCs (1.45 ± 0.17 kPa compared to 0.24 ± 0.07 kPa), and a 3-fold difference for the WKY (0.33 ± 0.14 kPa versus 0.09 ± 0.03 kPa). Similarly, the presence of hypertension introduced a 4-fold difference in the cellular elastic modulus compared to normotensive WKY at 18- weeks of age, and a 2 fold-difference at 5-weeks of age. These data also show that there is a heightened increase of cellular stiffness due to the combination of both older age and hypertension.

3.3.4 Ratio of Cellular to Matrix Elastic Moduli

The mean ± SEM ratio of the cellular to matrix elastic moduli for each strain-age combination is shown in Figure 3.16.

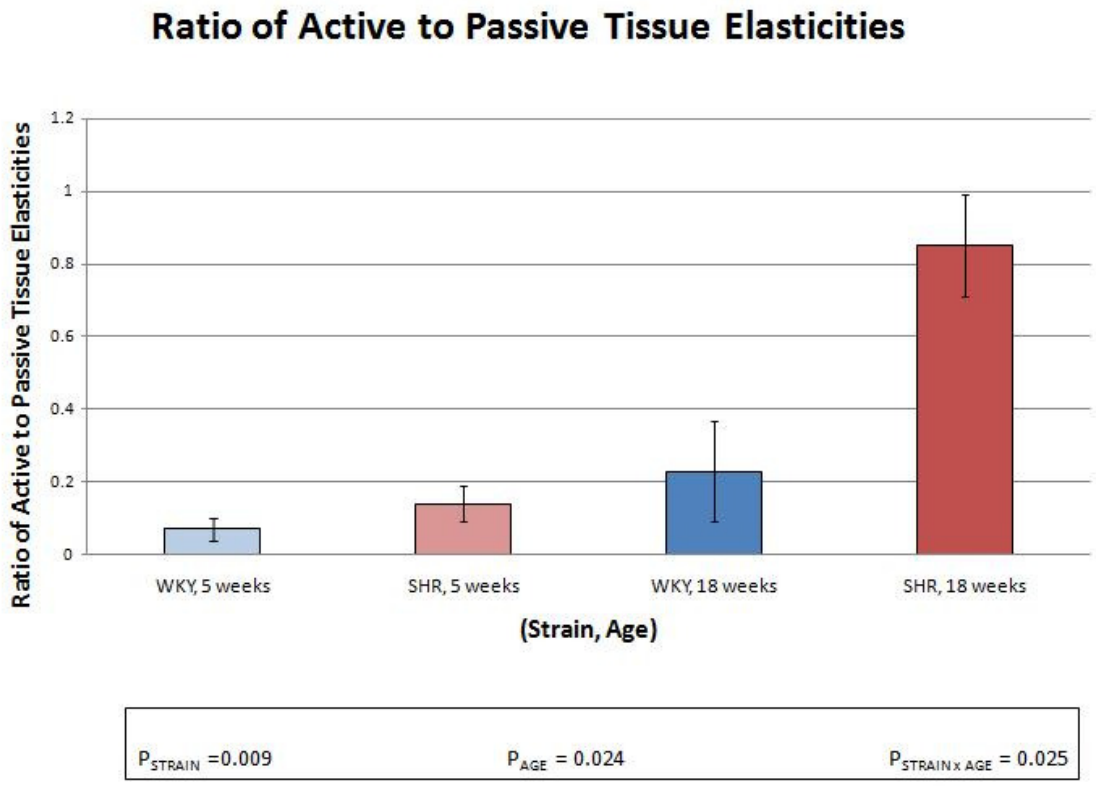

Figure 3.16 Mean ± SEM ratio of cellular to matrix elastic moduli.

These results show that, although significantly different for strain, age, and their interaction, the cellular elastic modulus was less than that of the matrix for each strain-age combination. With the exception of the 18-week SHR tissues, these ratios are considerably small.

3.3.5 Calculated Elastic Moduli Using an Alternative Cross-Sectional Area

The total tissue, matrix, and cellular moduli can also be computed using the alternative method to determine the baseline tissue cross-sectional area, as described earlier. In this method, twice the width and thickness of the tissue on the mandrel are used to estimate the baseline cross-sectional area. First it is assumed that the tissue is incompressible, and thus retains a certain volume while transferred off of the mandrel, and later loaded onto the mechanical testing apparatus. Approximating the shape of the tissue as two flat sheets, this volume on the mandrel given by the following equation,

$$\begin{aligned} V &= 2\,(width)_{mandrel}\,(thickness)_{mandrel}(length)_{mandrel} \\ &= (cross-sectional\ area)_{mandrel}\,(length)_{mandrel}\,, \end{aligned} \tag{3.1}$$

where the $(length)_{mandrel}$ is the circumference of the mandrel, 7.07 mm. Since a constant volume is assumed, this volume of the tissue ring at the baseline state is equivalent, and can be written as,

$$V = (cross-sectional\ area)_{baseline}(length)_{baseline}\,. \tag{3.2}$$

Since, $(length)_{baseline}$ is L_o (10.00 mm), the value of $(cross-sectional\ area)_{baseline}$ can be solved for in terms of known quantities.

$$(cross-sectional\ area)_{baseline} = \frac{(cross-sectional\ area)_{mandrel}(length)_{mandrel}}{(length)_{baseline}} \tag{3.3}$$

Using this alternative method of computation of the baseline cross-sectional area, the total tissue, matrix, and cellular elastic moduli can recalculated. These new values, as well their statistical significance, are compared to those obtained previously in Table 3.1.

Table 3.1 Computed Elastic Moduli Using the Original and Alternative Methods of Baseline Cross-Sectional Area Estimation

		Results Using ORIGINAL Cross-Sectional Area		Results Using ALTERNATIVE Cross-Sectional Area	
Total Tissue Elastic Modulus (kPa)	Strain-Age Combination	Mean	SEM	Mean	SEM
	WKY, 5-week	1.35	0.3	1.69	0.36
	SHR, 5-week	2.42	0.73	3.35	1.09
	WKY, 18-week	2.83	0.65	3.43	0.73
	SHR, 18-week	4.22	0.67	N/A	
	Statistical Analysis	$P_{strain} = 0.052$ $P_{age} = 0.012$ $P_{interaction} = 0.801$		$P_{strain} = 0.174$ $P_{age} = 0.054$	
Matric Elastic Modulus (kPa)	Strain-Age Combination	Mean	SEM	Mean	SEM
	WKY, 5-week	1.26	0.29	1.58	0.35
	SHR, 5-week	2.18	0.68	3.02	1.02
	WKY, 18-week	2.5	0.67	3.02	0.77
	SHR, 18-week	2.77	0.71	N/A	
	Statistical Analysis	$P_{strain} = 0.343$ $P_{age} = 0.151$ $P_{interaction} = 0.601$		$P_{strain} = 0.206$ $P_{age} = 0.113$	
Cellular Elastic Modulus (kPa)	Strain-Age Combination	Mean	SEM	Mean	SEM
	WKY, 5-week	0.09	0.03	0.11	0.04
	SHR, 5-week	0.24	0.07	0.33	0.1
	WKY, 18-week	0.33	0.14	0.4	0.16
	SHR, 18-week	1.45	0.17	N/A	
	Statistical Analysis	$P_{strain} < 0.0005$ $P_{age} < 0.0005$ $P_{interaction} = 0.001$		$P_{strain} = 0.060$ $P_{age} = 0.104$	
Ratio of Cellular to Matrix Elastic Moduli	Strain-Age Combination	Mean	SEM	Mean	SEM
	WKY, 5-week	0.07	0.03	0.07	0.03
	SHR, 5-week	0.14	0.05	0.14	0.05
	WKY, 18-week	0.23	0.14	0.23	0.14
	SHR, 18-week	0.85	0.14	N/A	
	Statistical Analysis	$P_{strain} = 0.009$ $P_{age} = 0.024$ $P_{interaction} = 0.025$		$P_{strain} = 0.266$ $P_{age} = 0.283$	

In the alternative method, the statistical computations were made from two sets of one-way ANOVA tests, where $p < 0.05$ was deemed significant. As such, the significance of strain was determined from comparisons of tissues containing 5-week, WKY and 5-week, SHR VSMCs. Additionally, the significance of age was computed from comparisons of 5-week, WKY and 18-week, SHR tissues.

Although computation using the alternative method did show similar trends to that which was obtained from the original method, it did not yield significant differences among the strain-age combinations in any of the tested categories. In fact, this suggests that these two methods of estimating the baseline cross-sectional area are not comparable.

As motivation for using the original method for baseline cross-sectional area determination, it should be noted that the alternative computations could only be done for those tissue rings that stayed on the mandrel. Thus, no 18-week, SHR tissues, which by the original method showed the greatest differences in elastic moduli, can be compared using this alternative method. Furthermore, it is questionable if the tissue rings can be assumed to be incompressible, as was done using the alternative method. While this may be an appropriate assumption for whole tissues, the tissue rings constructed were more gel-like. As a result, they could have absorbed or released medium as they were transferred from the mandrel to the baseline state. Thus, elastic moduli for this thesis were computed using the estimates for the baseline cross-sectional area described originally.

CHAPTER 4

DISCUSSION, FUTURE WORK, AND SUMMARY

4.1 Discussion

4.1.1 Interpretation of Elastic Moduli Differences

The results of this thesis showed significant differences amongst each strain-age combination for the total tissue and cellular elastic moduli, but not the matrix elastic moduli. It is interesting to note that the matrix elastic moduli was found to be dominant in all tissue groups. This is in contrast to the results of similar experiments (Wakatsuki et al., 2000), in which the cellular contribution was found to dominate.

This leads to an alternative model about how VSMCs behave in the reconstituted tissue rings. Initially, it was thought that the VSMCs contribute to the total tissue stiffness in parallel with the ECM, as modeled below in Figure 4.1

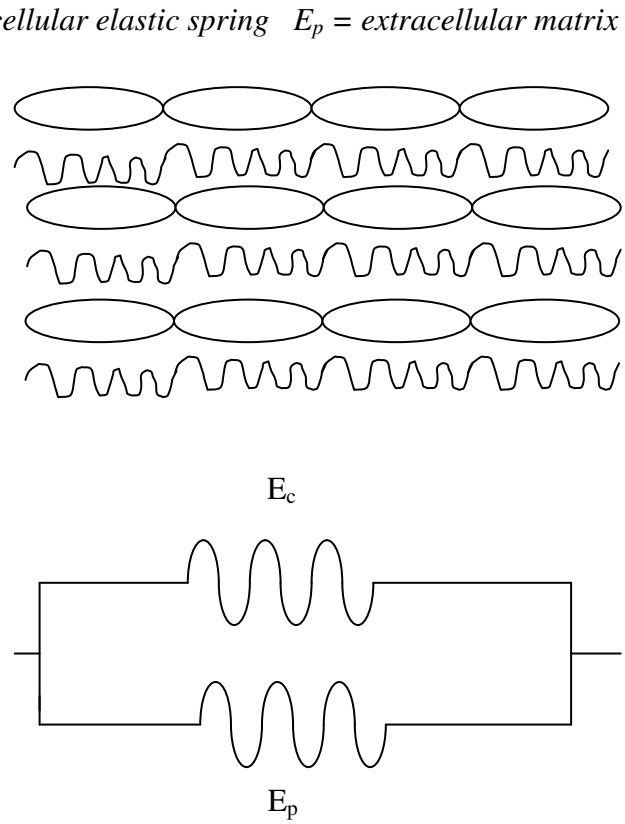

Figure 4.1 Original conceptual model of the reconstituted tissue rings. The VSMC and ECM spring elements act in parallel to produce the total tissue stiffness. Illustration courtesy of Dr. William C. Hunter.

This model is described by the following equations to produce the cellular component, E_c.

$$E_{total} = E_p + E_c$$

$$E_{total} - E_p = E_c \tag{4.1}$$

This model may be more representative of the *in vivo* aortic medial tissue environment, in which VSMCs may be tightly bound to the ECM proteins.

However, the in the reconstituted tissue rings, the density of VSMCs may be much less. In that case, a better model may entail the VSMCs acting in series with the ECM, which together also act in parallel with the ECM to produce the total stiffness component. This alternative model is presented below, in Figure 4.2.

E_c = cellular elastic spring E_{mc} = extracellular matrix spring connecting cells in series
E_p = extracellular matrix spring acting in parallel with cells-extracellular matrix in series

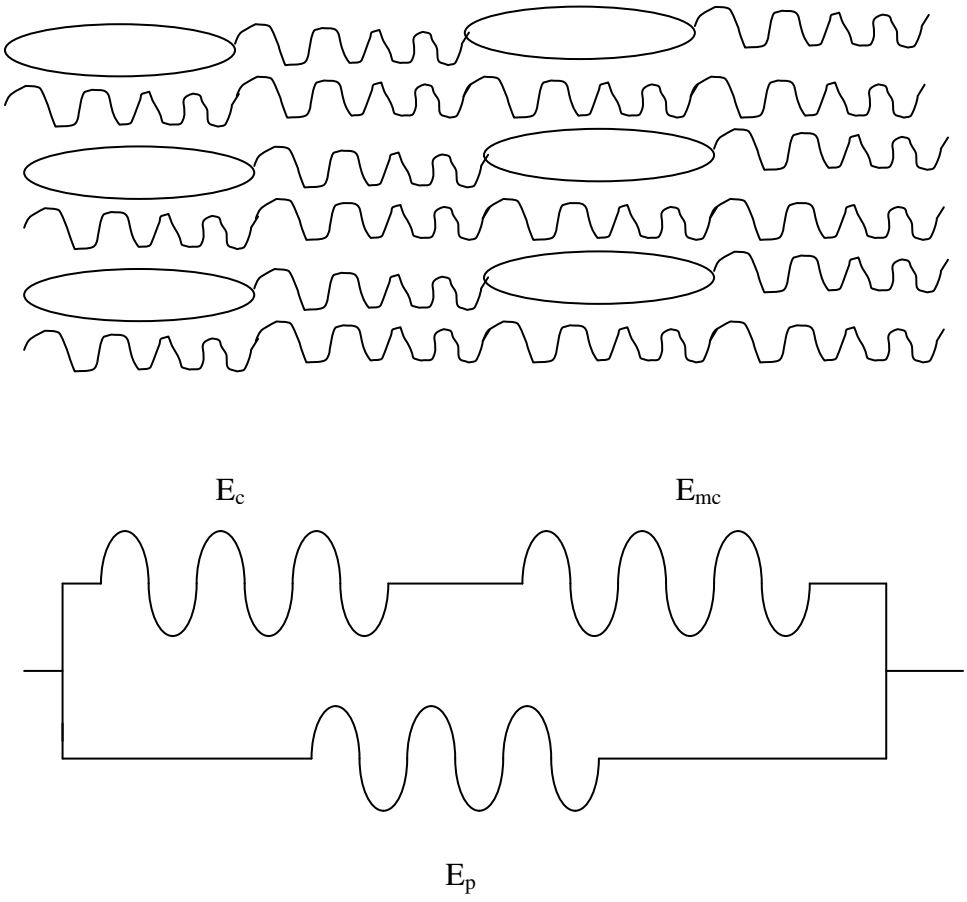

Figure 4.2 Alternative conceptual model of the reconstituted tissue rings. The VSMC spring acts in series with an ECM spring, which together act in parallel with an ECM spring. Illustration courtesy of Dr. William C. Hunter.

This model would then be described by the following equations, to determine the cellular component, E_c. Here, E_s is the series combination of springs E_c and E_{mc}.

$$\frac{1}{E_s} = \frac{1}{E_c} + \frac{1}{E_{mc}} \quad \text{which implies} \quad E_s = \frac{E_c\, E_{mc}}{E_c + E_{mc}}$$
$$E_{total} = E_s + E_p \tag{4.2}$$
$$E_{total} - E_p \;=\; E_s \;=\; E_c\left(\frac{E_{mc}}{E_c + E_{mc}}\right)$$

An analysis of this model indicates that this ratio, $\frac{E_{mc}}{E_c + E_{mc}} < 1$, except in cases where the extracellular matrix is much stiffer than the cellular component, E_c. In these cases, the fraction $\frac{E_{mc}}{E_c + E_{mc}} \approx 1$. This would simplify to the original conceptual model, described above.

The important implication of this alternative conceptual model is that the observations recorded for the "cellular" component of the tissue rings are an underestimate of the true cellular component, E_c.

4.1.2 Comparison to VSMC Elastic Moduli Found in Other Works

In fact, the determined cellular elastic moduli found in these experiments are much less those found in other studies. Similar experiments with non-human primate VSMCs have reported values on the order of 10 times greater than what was found in this work (Qiu et al., 2010). However, this may due to fact that those experiments were carried out at larger values of L_0. In fact, our own preliminary experiments done for this thesis demonstrated much smaller active elasticities at smaller L_0 values. Other estimates of

single cell VSMC elasticities have ranged from 0.001 MPa to 6.8 MPa and tissue elasticities of 0.017 to 375 MPa (Wakatsuki et al., 2000).

4.1.3 The Effect of the Mandrel in Tissue Remodeling

Changes in the dimensions of the tissue rings were observed during the VSMC remodeling of the collagen. To summarize, the thickness dramatically decreased, while the width and lengths moderately elongated.

In particular, a significant difference was found in the unloaded lengths of the tissue rings between strain-age combinations. The results suggest that the younger, normotensive VSMC-containing were under greater circumferential compression on the mandrel than their counterparts. The fact that the tissues containing the older-SHR VSMCs consistently slipped off the mandrel may be related to their relatively small circumferential compression.

An interesting point to consider in evaluating this experimental approach is the role of tissue-mandrel interactions had in this remodeling process. This is particularly important, as the tissues containing the 18-week SHR VSMCs would have had much less interaction with the mandrel. It can be assumed that in the other groups of tissues, a significant mandrel interaction was present after incubation, based on the noted width and length extensions of the tissues on mandrel compared to their unloaded widths, as shown in Figures 3.6 and 3.7.

Suppose that the tissue-mandrel interaction negatively influenced the VSMC-collagen remodeling through an additional compressive stress in the radial direction. Perhaps, this may be due to an attraction of the VSMCs to the mandrel. Thus, throughout

the dynamic remodeling process, the effective remodeling was the difference in the true VSMC-collagen remodeling and the radial pull of the mandrel.

$$\text{“Effective Remodeling”} = \text{“True Remodeling”} - \text{“Mandrel Pull”} \quad (4.3)$$

Comparisons of the “Effective Remodeling” and the “Mandrel Pull” would be informative in evaluating the cylindrical molds used for tissue formation. A relatively small “Mandrel Pull” compared to the “Effective Remodeling” would be indicative that this “Mandrel Pull” did not significantly affect tissue formation. In that case, it should not matter too much that the 18-week SHR tissue did not stay on the mandrel. However, a relatively large “Mandrel Pull” could be indicative of a bias in the tissue remodeling containing the 18-week SHR VSMCs. However, it is uncertain as to how to estimate these values. The important supposition in this analysis there are two major factors that could influence tissue formation – the intended VSMC-collagen interaction, as well as the effect of the mandrel.

4.2 Future Work

Additional analysis could be done to further characterize the elastic moduli of VSMCs. For instance, a more sophisticated analysis could be done to determine the peak force produced during the stress-relaxation, as well as the time constant of the viscoelastic response. Also, experiments using the VSMCs from more rats in each strain-age combination could be done to see if these results are consistent across large populations. Furthermore, a method to determine the effect of the mandrel during incubation could be developed.

However, the dramatic differences found in VSMC elasticities obtained using the reconstituted tissue model motivate further exploration as to the cause of the differences in the cell populations studied. Additional studies of the likely sub-cellular differences could be made using AFM to study the forces exerted by individual cells. These may allow for a better understanding of the molecular basis for differences in elastic moduli.

Finally, these experimental results support the reconstituted tissue model as rough method of determining cellular elastic moduli. This technique could be employed to study the potential cellular contribution of VSMCs that differ in other factors relating to aortic stiffness. These include gender comparisons using female SHR, and difference induced by diet using the Dahl/Salt Sensitive rats (DSS). Finally, VSMCs from different regions of the aorta may be studied, including the abdominal aorta, to investigate if these cellular differences are prevalent throughout the systemic circulation.

4.3 Summary

In this thesis, the potential contribution of VSMCs to aortic stiffness was studied. This was attempted by estimating the collective cellular elastic moduli of populations of VSMCs obtained from rats that differed in two characteristics that affect aortic stiffness: hypertension and aging.

To measure the elastic moduli of the VSMCs, a reconstituted tissue model was developed to test its mechanical properties through stress-relaxation testing. The force recordings from these uni-axial stretch measurements were used to determine the total elastic moduli, and indirectly the cellular contribution after pharmacological disruption of the actin cytoskeleton with cytochalasin D.

The results showed significant differences in the cellular elastic moduli computed for the VSMCs from each strain-age combination of rat. In particular, the VSMCs cells from the older SHR were found to be several magnitudes stiffer that their same-age normotensive control, WKY, as well as the younger SHR. These findings indicate that VSMC stiffness is heightened with age and hypertension. It is possible that this greater VSMC stiffness could contribute to the increased aortic stiffness found in hypertension and aging.

APPENDIX A

MATLAB CODE

The MATLAB code used to obtain the baseline and steady-state force readings is shown below.

```
% This script loads the Notochord force data, filters the data, and
outputs
% the baseline and steady-state forces.

data = load('s2.txt');  % Input name of .txt file

Fs = 500;       % Sampling frequency (Hz)
Fc = 4;         % Cutoff frequency (Hz)
order = 4;      % Filter order

time = 0:(1/Fs):((length(data)-1)*(1/Fs)); %Creates time vector

% Plots raw data
figure;
plot(time, data)
xlabel('Time (s)')
ylabel('Force (mg)')
title('RAW Force Recordings during a 10% Stretch')

% Filters the data and plots the result
[B, A] = butter(order, 2*Fc/Fs);  % Obtains filter coefficients

figure;
filtered_data = filtfilt( B, A, data);
plot(time, filtered_data)
xlabel('Time (s)')
ylabel('Force (mg)')
title('FILTTERED Force Recordings during a 10% Stretch')

% Computes Average Baseline and Steady-State Forces
[max_val, index_max] = max(filtered_data);
time_max = index_max*(1/Fs);

% Finds times of begininng and end of averaging periods
upper_baseline_time = time_max - 5;
lower_baseline_time = time_max - 25;
lower_steadystate_time = time_max + 90;
upper_steadystate_time = time_max + 110;

% Finds indicies of those times
upper_baseline = upper_baseline_time/(1/Fs);
lower_baseline = lower_baseline_time/(1/Fs);
lower_steadystate = lower_steadystate_time/(1/Fs);
```

```
upper_steadystate  = upper_steadystate_time/(1/Fs);

% Outputs baseline and steady-state force averages
baseline_average =
sum(filtered_data(lower_baseline:upper_baseline))/(upper_baseline -
lower_baseline)
steadystate_average =
sum(filtered_data(lower_steadystate:upper_steadystate))/(upper_steadyst
ate - lower_steadystate)
```

APPENDIX B

DIMENSIONAL AND FORCE DATA USED FOR CALCULATIONS

Table B.1 to B.3 show the data used for calculations.

Table B.1 Dimensions of the tissue rings

Animal Type	Tissue Ring	Width on Mandrel (mm)	Width off Mandrel (mm)	Thickness (mm)	Length off Mandrel (mm)
WKY, 5-weeks	1	9.04	8.92	0.15687	7.27
	2	12.80	11.34	0.15687	8.03
	3	12.59	9.8	0.15687	7.74
	4	12.39	10.5	0.15687	8.29
	5	12.22	10.36	0.15687	8.65
	6	11.75	11.5	0.15687	9.03
	7	10.68	10.16	0.15687	7.83
SHR, 5-weeks	1	12.8	11.34	0.15687	7.13
	2	8.51	9.47	0.15687	7.37
	3	11.49	10.74	0.15687	7.17
	4	11.4	9.82	0.15687	7.05
	5	10.84	10.13	0.15687	7.97
	6	11.05	10.3	0.15687	8.01
	7	11.9	10.94	0.15687	8.08
WKY, 18-weeks	1	11.66	9.81	0.15687	7.69
	2	11.48	9.39	0.15687	7.72
	3	11.53	9.58	0.15687	8.07
	4	11.99	11.06	0.15687	7.8
	5	11.46	10	0.15687	7.52
	6	11.95	10.93	0.15687	7.88
	7	11.33	9.98	0.15687	8.12
SHR, 18-weeks	1	N/A	10.63	0.15687	7.38
	2	N/A	10.67	0.15687	7.28

3	N/A	9.76	0.15687	7.22
4	N/A	9.73	0.15687	7.06
5	N/A	7.6	0.15687	7.08
6	N/A	9.72	0.15687	7.11
7	N/A	9	0.15687	7.08

Table B.2 Force Values for the Third Stretch of the Tissue Rings

		L0 = 10 mm, 10% strain (delta L = 1 mm)		
		Third Stretch		
Animal Type	**Tissue Ring**	**Baseline Force (mg)**	**Steady-State Force (mg)**	**Net Force (mg)**
WKY, 5-weeks	1	11.4941	23.2941	11.8
	2	-3.7482	94.1923	97.9405
	3	52.4006	113.5398	61.1392
	4	104.2795	148.4987	44.2192
	5	-27.8217	-8.1111	19.7106
	6	78.0119	121.7669	43.755
	7	32.3779	73.9783	41.6004
SHR, 5-weeks	1	10.7041	77.697	66.9929
	2	-13.6201	138.2524	151.8725
	3	36.9235	221.4595	184.536
	4	53.1111	105.6403	52.5292
	5	2.0274	27.2715	25.2441
	6	22.6262	65.1244	42.4982
	7	19.0254	53.7153	34.6899
WKY, 18-weeks	1	178.1141	322.9771	144.863
	2	21.1991	196.6775	175.4784
	3	102.7371	167.4027	64.6656
	4	-9.6433	35.745	45.3883
	5	45.876	97.0668	51.1908
	6	-33.0805	44.2251	77.3056
	7	-11.5471	56.6452	68.1923
SHR, 18-weeks	1	49.6636	166.357	116.6934
	2	120.2037	349.4541	229.2504
	3	-8.7256	111.4965	120.2221
	4	47.3161	118.4289	71.1128
	5	13.5482	167.532	153.9838
	6	78.15	191.3574	113.2074
	7	-98.9451	-17.0566	81.8885

Table B.3 Force Values for the Fourth Stretch of the Tissue Rings

		L0 = 10 mm, 10% strain (delta L = 1 mm)		
		Fourth Stretch		
Animal Type	**Tissue Ring**	**Baseline Force (mg)**	**Steady-State Force (mg)**	**Net Force (mg)**
WKY, 5-weeks	1	3.8463	15.2831	11.4368
	2	-16.5832	79.1879	95.7711
	3	47.3261	105.626	58.2999
	4	111.1318	146.4908	35.359
	5	-42.0922	-22.4881	19.6041
	6	76.4343	116.8509	40.4166
	7	28.4664	67.5999	39.1335
SHR, 5-weeks	1	9.3036	69.903	60.5994
	2	-11.0267	130.9924	142.0191
	3	33.0869	197.8122	164.7253
	4	49.4184	100.3965	50.9781
	5	0.2504	25.1989	24.9485
	6	26.9505	58.5991	31.6486
	7	22.7225	49.39	26.6675
WKY, 18-weeks	1	133.7004	278.0594	144.359
	2	16.5997	180.3236	163.7239
	3	124.753	156.0882	31.3352
	4	-11.4726	30.5551	42.0277
	5	43.7833	90.7383	46.955
	6	-28.6841	33.1582	61.8423
	7	-13.1585	49.9089	63.0674
SHR, 18-weeks	1	41.6058	108.2794	66.6736
	2	122.656	332.8414	210.1854
	3	10.3616	88.5242	78.1626
	4	45.7354	77.515	31.7796
	5	11.1688	116.9907	105.8219
	6	77.4328	152.6489	75.2161
	7	-105.661	-78.3348	27.3262

REFERENCES

Bell, E., B. Ivarsson, and C. Merrill. (1979). Production of a tissue-like structure by contraction of collagen lattices by human fibroblasts of different proliferative potential in vitro. *Proceedings from the National Academy Sciences, U.S.A,* 76:1274 –1278.

Chamiot-Clerc, P., Renaud J.F., Safar, M.E. (2001). Pulse Pressure, Aortic Reactivity, Endothelium Dysfunction in Old Hypertensive Rats. *Hypertension*, 37:313-321.

Charles River Laboratories, Inc. *Spontaneously Hypertensive Rats*. Retrieved on December 27, 2010, from http://www.criver.com/EN-US/PRODSERV/BYTYPE/RESMODOVER/RESMOD/Pages/SHRRat.aspx.

Eschenhagen, T., C. Fink, U. Remmers, H. Scholz, J. Wattchow, J. Weil, W. Zimmermann, H. H. Dohmen, H. Schafer, N. Bishopric, T. Wakatsuki, and E. L. Elson. 1997. Three-dimensional reconstitution of embryonic cardiomyocytes in a collagen matrix: a new heart muscle model system. *Faseb J.* 11:683– 694.

Griffith, L.G., Swartz, M.A. (2006). Capturing complex 3D tissue physiology in vitro. *Nature Reviews. Molecular Cell Biology*, 7:211-224.

Grinnell, F. (1994). Fibroblasts, myofibroblasts, and wound contraction. *Journal of Cell Biology,* 124:401– 404.

Holzapfel, G.A., Gasser, T.C., Ogden, R.W. (2000). A new constitutive framework for arterial wall mechanics and a comparative study of material models. *Journal of Elas*ticity, 61: 1-48.

Lanzer, P., Topol, E.J. (2002). *Pan vascular medicine: integrated clinical management*. New York, NY: Springer.

Lerman, L.O., Chade, A.R., Sica, V., and Napoli, C. (2005). Animal models of hypertension: An overview. *Journal of Laboratory and Clinical Medicine*. 146:160-173.

Luo, Y., Owens, D., Mulder, G., McVey, A., Fisher, T. (2008). *Blood Pressure Characterization of Hypertensive and Control Rats for Cardiovascular Studies*. Retrieved on December 27, 2010, from http://www.criver.com/SiteCollectionDocuments/rm_rm_r_08_bp_characterization_of_hypertensive_and_cardiovascular_studies.pdf.

Marque, V., Kieffer, P., Atkinson, J., Lartaud-Idjouadiene, I. (1999). Elastic Properties and Composition of the Aortic Wall in Old Spontaneously Hypertensive Rats. *Hypertension*, 34:415-422.

Marquez J.P., Elson E.L., Genin G.M. (2010). Whole cell mechanics of contractile fibroblasts: relations between effective cellular and extracellular matrix moduli. *Philosophical transactions. Series A, Mathematical, physical, and engineering sciences*, 368:635-654.

Mitchell, G.F. (2009). Arterial Stiffness and Wave Reflection: Biomarkers of Cardiovascular Risk. *Artery Research*, 3:56-64.

Nagendra, Shilpa. (2010). *Stiffness of vascular smooth muscle cells from aged primates measured using reconstituted tissue model* (Master's thesis). New Jersey Institute of Technology, Newark, NJ.

Nichols, W.W., O'Rourke, M.F. (1998). *MacDonald's Blood Flow in Arteries*, 4th ed. London, UK: Arnold, Hodder Headline Group.

O'Rourke, M.F. (2006). Principles and definitions in arterial stiffness, wave reflection and pulse pressure. In Safar, M., O'Rourke, M.F (Eds.) *Arterial stiffness in hypertension*, (pp. 3-19). Amsterdam, the Netherlands: Elsevier B.V.

Okamoto, A.K. (1963). Development of a strain of spontaneously hypertensive rat. *Japanese Circulation Journal*; 27:282-293.

Palsson, B.Ø., Bhatia, S.N. (2004). *Tissue Engineering*. Upper Saddle River, NJ: Pearson Education, Inc.

Rao, S.S., Winter, J.O. (2009). Adhesion molecule-modified biomaterials for neural tissue engineering. *Frontiers in Neural Engineering*, 2: Epub 2009 June 9.

Safar, M., Chamiot-Clerc, P., Dagher, G., Renaud J.F. (2001). Pulse Pressure, Endothelium Function, and Arterial Stiffness in Spontaneously Hypertensive Rats. *Hypertension*; 38:1416-1421.

Safar, M.E., Boudier, H.S. (2005). Vascular Development, Pulse Pressure, and the Mechanisms of Hypertension. *Hypertension*, 46:205-209.

Safar, M., Frohlich, E.D. (2007). *Atherosclerosis, larger arteries and cardiovascular risk*. Basel, Switzerland: S. Karger AG.

Santelices, L.C., Rutman, S.J., Prantil-Baun, R., Vorp, D.A., Ahearn, J.M.. (2008). Relative contributions of age and atherosclerosis to vascular stiffness. *Clincial Translational Science*, 1: 62-66.

Spina, M., Garbisa, S., Hinnie, J., Hunter, J.C., and Serafini-Fracassini, A. (1983). Age-related changes in composition and mechanical properties of the tunica media of the upper thoracic human aorta. *Arteriosclerosis*, 3:64-76.

Storr, W. *Butterworth Filter Design*. Basic Electronics Tutorials. Retrieved January 6, 2011, from http://www.electronics-tutorials.ws/filter/filter_8.html.

Sun, Z., Martinez-Lemus, L.A., Trache, A., Trzeciakowski, J.P., Davis, G.E., Pohl, U., Meinenger, G.A. (2005). Mechanical properties of the interaction between fibronectin and $\alpha_5\beta$-1 integrin on vascular smooth muscle cells studied using atomic force microscopy. *American journal of physiology. Heart and circulatory physiology*, 289: H2526-35.

Qiu, H., Zhu, Y., Sun, Z., Trzeciakowski, J.P., Gasner, M., Depre,C., Resuello, R.R.G., Natividad, F.F., Hunter, W.C., Genin, G.M., Elson, E.L., Vatner, D.E., Meininger, G.A., Vatner, S.F. (2010). Vascular smooth muscle cell stiffness as a mechanism for increased aortic stiffness with aging. *Circulation Research*, 107:615-619.

Wakatsuki, T., Kolodney, M.S., Zahalak, G.I., and Elson, E.L. (2000). Cell mechanics studied by a reconstituted model tissue. *Biophysics Journal*, 79:2353-2368.